Effect of damage on vibration characteristic of FDM printed lattice structure material

Muhamad Syafwan Azmi[1], Rainah Ismail[1,2,*], Rafidah Hasan[1,2], Azma Putra[1,2], Muhammad Nasruddin Nurdin[1]

[1)] Fakulti Kejuruteraan Mekanikal, Universiti Teknikal Malaysia Melaka,
Hang Tuah Jaya, 76100 Durian Tunggal, Melaka, Malaysia
[2)] Centre for Advanced Research on Energy, Universiti Teknikal Malaysia Melaka,
Hang Tuah Jaya, 76100 Durian Tunggal, Melaka, Malaysia

[*]Corresponding e-mail: rainah@utem.edu.my

Keywords: Lattice structure; vibration analysis; damage

ABSTRACT – The aims of this study are to investigate the effect of damage extent and damage location on natural frequencies of the BCC lattice bar. The bar samples were fabricated by using fused deposition modeling (FDM) additive manufacturing (AM) technique. The damage is represented by missing lattice unit cells within the structure. Findings show that natural frequency values decrease with the increase of damage extents. Meanwhile, the natural frequency values increase as the damage location became farther from the clamped edge. This research provides good information on the influence of damage existence to the natural frequency values of the lattice structure.

1. INTRODUCTION

Damage is defined as alteration introduced into a system in which will affect the way of that system behaves in term of its performance. Structural damage detection has been one of the main popular concerns in scientific community as many incidents that have caused human loses such as airplane crashes or collapsed bridges or buildings [1]. The types of damage that can happen in structures are cracks, delamination and deformations due to fatigue from constant exposure to the uncontrol vibration. Presence of damage can lead to unwanted instances of high vibration that can cause long-term and short-term damaging effects on the structure's integrity. This phenomenon is extremely dangerous as structures cannot function as designed which can then ultimately fail. Failure of a structure can result in dreadful consequences such as loss of life as evidently happened from collapsed buildings during earthquake. Hence, damage detection to the structure at the initial stage of research and development can provide insight into the real behavior of the system, evaluate its performance, suitability, limitations and this in due course can provide better safety of the structure in real dynamic applications. For this reason, various effect of damages on vibration characteristics of the lattice core material sandwich structures numerically using experimentally validated FEM models are explored [2,3]. Therefore, this study attempted to investigate the effects of damage extent and damage location on the natural frequency values of the lattice structures experimentally in order to correlate the findings. The hypothesis that will be tested are that larger the damage area and the closest damage region to the boundary condition will have higher effect on the natural frequency values of the lattice bars.

2. METHODOLOGY

2.1 Sample Preparation

Lattice bar samples with dimension of 160mm x 30mm x 15mm size were made by using the FDM AM. The strut diameter of the BCC lattice bars was kept at 1.8 mm with standard print quality mode combination [4]. The damage extent is represented by using a damage parameter η.

$$\eta = \frac{n}{N} \quad (1)$$

Where n is the number of missing unit cells and N is total unit cells of the intact lattice bar sample. For damage extent study, different damage parameters ranging from η =0.00 (intact) to η =0.50 were used with all damage location starting near the clamped edge boundary condition as illustrated in Figure 1. Meanwhile for damage location study, damage extent was kept at damage parameter η =0.02 and the damaged region was set to be at the clamped edge, at the opposite free end or in between them as illustrated in Figure 2.

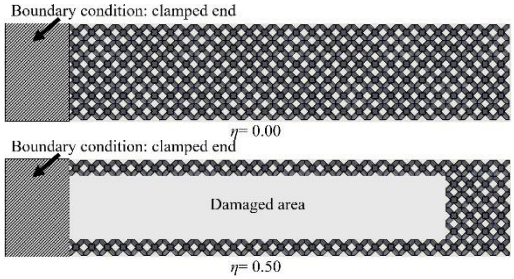

Figure 1 Illustration of lattice bar with different damage extent (top view).

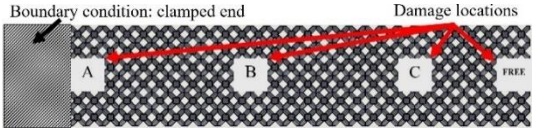

Figure 2 Illustration of the lattice structure's damage location (top view).

2.2 Vibration Testing

The experimental setup for vibration testing consists of Dataphysics Quattro as signal generator and analyzer, accelerometer sensor, force sensor, shaker, signal amplifier and fabricated test rig to clamp the bar samples was used. Details of the vibration testing procedure and schematic experimental set-up is available in previous study [4]. The measurement points and excitation point are as illustrated in Figure 3.

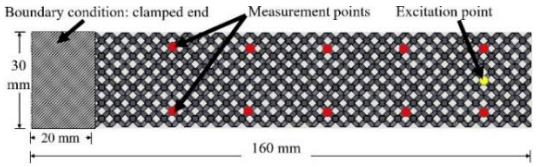

Figure 3 Excitation and measurement point locations (top view).

3. RESULTS AND DISCUSSION

3.1 Effect of Damage Extent

The effects of damage extents on the first two natural frequencies are displayed in Figure 4. Based on Figure 4, it can be seen from the trendline, generally that the influence of damage to the natural frequency values increase with the increase in the damage parameter. The natural frequency values decrease due to loss of stiffness caused by damage present in the lattice bars [2]. The percentage different of the natural frequency for the first and second modes of vibration are 17.56 % and 9.56% respectively. This shows that the influence of damage extent was greater for the first mode natural frequency.

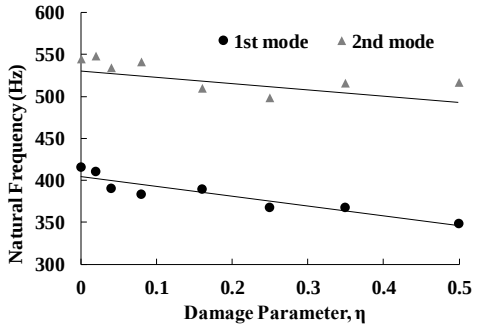

Figure 4 Effect of damage extents on the natural frequency values.

3.2 Effect of Damage Locations

Figure 5 shows the effects of damage locations on the first two natural frequencies. It can be seen from Figure 5 that both natural frequency values increase as the damage location became farther from the clamped edge. This indicates that the effect of damage on the natural frequencies become smaller as the damage zone moves from clamped edge boundary condition to the free end. This behavior is due to more flexibility at the free end of the lattice bar samples. A similar finding was obtained by Lou et al., (2014) and Li et al., (2015) numerically [2-3]. From Figure 5, only first mode natural frequency at the location A shows lesser natural frequency value as compared to that of the intact lattice bar. This shows that loss of stiffness was more significant when the damage is closest to the boundary condition. On the other hand, at the location B, C and 'Free', higher natural frequency values can be observed. This phenomenon is believed to be due to lower mass value with less effect to the stiffness of the lattice bar samples. This is proven especially by result at the location 'Free' where stiffness was not affected by the existence of damage as the lattice bar sample was excited before the damage location 'Free'. However, the mass of the lattice bar sample at the location 'Free' was lower as compared to that of the intact lattice bar. Based on equation (2), the natural frequency is inversely proportional to mass. Therefore, lower mass would increase the natural frequency values.

$$\omega_n = \sqrt{\frac{k}{m}} \tag{2}$$

Where ω_n is the natural frequency [Hz], k is the stiffness [N/m] m is the mass [kg] l is the length of the lattice bar [m]

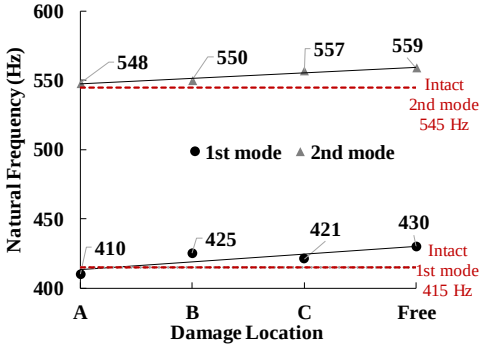

Figure 5 Graph of natural frequency values against damage location.

4. CONCLUSIONS

The effect of artificial damage on the lattice bar samples were studied experimentally. In the damage extent study, it was found that the natural frequency values decrease with the increase of damage parameter. On the other hand, for damage locations study, it was found that the natural frequency values increase as the distance of damage to the boundary condition became far. The findings indicated that the damage zone should be placed far away from the clamped edge and small when embedding additional component such as screw or motor in the real applications of lattice structures bar so that natural frequency can be decreased by smaller extents.

ACKNOWLEDGMENT

This research was fully funded by research grant FRGS/1/2016/TK03/FKM-CARE/F00316 provided by Ministry of Education Malaysia. All equipment's used for specimens' fabrication and testing are provided by Universiti Teknikal Malaysia Melaka.

REFERENCES

[1] Sampaio, R. P. C., Maia, N. M. M., & Silva, J. M. M. (1999). Damage detection using the frequency-response-function curvature method. *Journal of sound and vibration*, *226*(5), 1029-1042.

[2] Lou, J., Wu, L., Ma, L., Xiong, J., & Wang, B. (2014). Effects of local damage on vibration characteristics of composite pyramidal truss core sandwich structure. *Composites part b: Engineering*, *62*, 73-87.

[3] Li, B., Li, Z., Zhou, J., Ye, L., & Li, E. (2015). Damage localization in composite lattice truss core sandwich structures based on vibration characteristics. *Composite Structures*, *126*, 34-51.

[4] Azmi, M. S., Ismail, R., Hasan, R., Alkahari, M. R., & Tokoroyama, T. (2017). Vibration analysis of FDM printed lattice structure bar. *Proceedings of SAKURA Symposium on Mechanical Science and Engineering*, 33-35.

Wireless control of two wheels self-balancing robot using arduino microcontroller

Nurul Muthmainnah Mohd Noor*, Ahmad Nurussalam Yusof

Fakulti Kejuruteraan Mekanikal, Universiti Teknologi MARA, Cawangan Pulau Pinang, Kampus Permatang Pauh, 13500 Permatang Pauh, Pulau Pinang, Malaysia

*Corresponding email: muthmainnah@uitm.edu.my

Keywords: Inverted pendulum, two wheels self-balancing robot, gyroscope

ABSTRACT – This paper presents the design and implementation of two wheels self-balancing robot based on the concept of inverted pendulum. A small two-wheel balancing robot using a mobile robot kit is designed with ability to balance the upright position on the level landscape. The route of movements of the robot are controlled by wireless condition through Bluetooth. To balance the platform, the sensor which called MPU is used to detect the tilt angle of the robot by using Kalman Filter algorithm. Lastly, the results show that the wireless control system of the robot using Arduino microcontroller meets its objective.

1. INTRODUCTION

The working principle of the two wheels balancing robot is really straightforward. The robot will try to drive its wheels in the direction where the upper part of the robot body is falling to maintain the position of wheels under the centre of gravity and then achieve the balancing effect [1]. Regularly, the two wheels self-balancing robot is planned based on the inverted pendulum idea which has been considered or investigated seriously by many research education institutes and business organizations. As the outcome, balancing robots that fill different needs have been developed. The most conspicuous case is the Segway Human Transporter by the Segway Company which has been marketed as transportation for humans [2].

The fundamental of the controller is to use the wheel encoder, gyroscope and accelerometer sensors to estimate the state of mind of the platform and after that to utilize this data to drive their activity wheel in the direction to keep up an upright and balanced position platform [3]. It implies to continue falling off away from the vertical axis, and then a gyro chip is expected to give the point position of the inverted pendulum or robot base and input into the controller. The Arduino controller will give a sort of feedback signal through MPU sensor to turn the stepper motor clockwise or anticlockwise, along these lines balancing the platform. These two estimations are summed and fed-back to the stepper motor which delivers the counter torque required to balance the platform robot.

In contrast with the two wheels balancing robot, the traditional three or four wheels' robots have a few limitations. These robots are steady when static yet effectively to be precarious in dynamic condition because of too high centre point of gravity or too quick changing movement of the robots. In this circumstance, the robots have high probability to topple during movement.

This paper is organized as follows: Section 2 describes the methodology of robot; Section 3 presents the implementation and results followed by some conclusion in last section.

2. METHODOLOGY

The methodology is a list of actions need to do in order to accomplish the self-balancing robot. There are three main parts involved; design prototype, circuit for sensor and implementation prototype with circuit. The sensor circuit was required to control the stepper motor. The prototype of the self-balancing two wheels also was constructed based on the designing using CATIA. This was followed by software algorithm implementation and hardware integration. Finally, the model was tested and fine-tuned for performance improvement. Figure 1 shows the balancing robot.

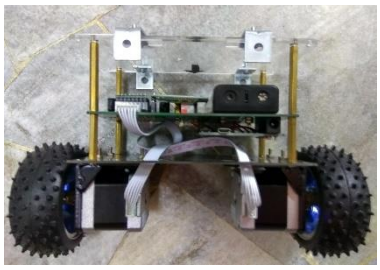

Figure 1 Balancing robot.

2.1 Circuit Design Construction

The fundamental segments in the circuit of the self-balancing robot are the multi-purpose unit (MPU), Arduino Leonardo, the stepper motor driver and the Bluetooth module. Arduino Leonardo R3 is acted as a module for control unit to handle the peripherals of the robot. The MPU6050 as a gyro sensor is utilized to quantify both accelerometer and gyroscope. Kalman Filter in programming is to obtain the tilt angle of the robot. After that, the obtained tilt angle is sustained into PID controller that compensates error between the actual tilt angle and the desired tilt angle and afterward controls the robot correspondingly for balancing purpose. The Bluetooth Module, HC-06 goes about as the wireless communication platform between the Arduino Mainboard and the Android Smartphone. Through this module, the development of the robot is controlled physically in wireless condition through an Android Smartphone. The stepper motor driver, A4988 is utilized to drive the robot stepper motors which control the development of the robot.

2.2 Hardware Design Construction

In this project, the hardware and mechanism of the balancing robot is crucial as it requires accurate measurement and symmetrical design in order for the robot to balance nicely. Much thought must be considered, for example, the torque of the stepper motor; the height of the robot is 13cm and the centre of gravity of the robot. Figure 2 shows the robot structure that designed using CATIA software.

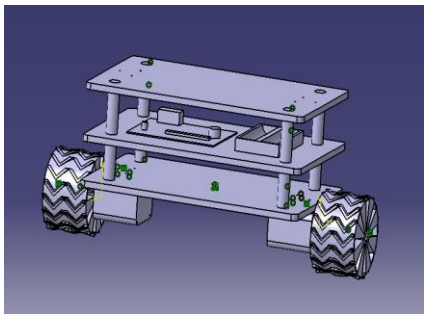

Figure 2 CATIA drawing of the robot structure.

2.3 Software Algorithm

The software algorithm and coding is certainly the most difficult and time consuming part. It involves the programming of the microcontroller to perform the desired task, to receive and process inputs from sensors and to produce correct and accurate output to control the stepper motor.

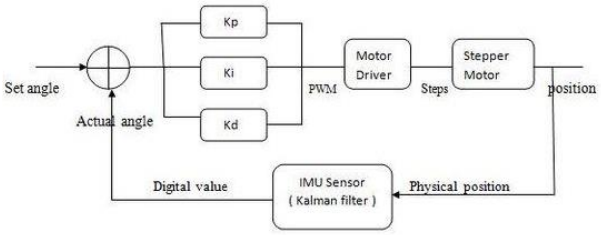

Figure 3 Block diagram for self-balancing robot.

Figure 3 shows a basic block diagram for the balancing robot. The desired set point is the angle that allows the robot to balance in upright position, while the actual tilt angle is the instantaneous angle of the robot as the robot try to balance. The actual tilt angle is measured by the IMU and the Kalman Filter is used to produce a more stable angle measurement and this angle is deducted from the desired set point. From there, an error, which is the difference between the desired and actual tilt angle is obtained and is it is fed into PID controller. The PID controller will then generate the appropriate speed output to control the stepper motors in order to balance the robot.

3. RESULTS AND IMPLEMENTATION

In this section, the working of self-balancing robot will be discussed. Figure 4 shows the control circuit of the robot. The Bluetooth module establishes a wireless connection between Arduino and android application to control robot movement manually for navigation in wireless condition. The implementation of the Kalman Filter and the PID controller making it balances nicely on the flat surfaces. Therefore, Figure 5 shows the robot balancing on flat surfaces.

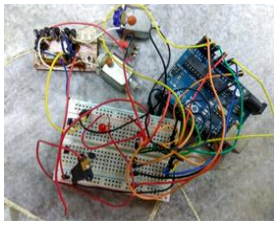

Figure 4 Controller circuit for robot.

Figure 5 Robot balancing on flat surfaces.

4. CONCLUSION

The project has successfully met the objectives to design using CATIA and ready to balance at its upright position on the level surfaces by using the wireless condition for navigation. The next future, the fuzzy logic controller also can be implemented to provide better performance in balancing.

ACKNOWLEDGEMENT

This paper is contributed with Universiti Teknologi MARA cawangan Pulau Pinang.

REFERENCES

[1] Juang, H. S., & Lurrr, K. Y. (2013). Design and control of a two-wheel self-balancing robot using the arduino microcontroller board. In *2013 10th IEEE International Conference on Control and Automation (ICCA)* (pp. 634-639).

[2] Anderson, D. P. (2016) nBot balancing robot. Available online: http://www.geology.smu.edu/ dpa-www/robo/nbot.

[3] An, W., & Li, Y. (2013). Simulation and control of a two-wheeled self-balancing robot. In *2013 IEEE International Conference on Robotics and Biomimetics (ROBIO)* (pp. 456-461).

The assessment of vibration level among female passengers in Malaysia KTM commuter

Fatimah Abdullah[1,*], Wan Hasrulnizzam Wan Mahmood[2], Seri Rahayu Kamat[1]

[1)] Fakulti Kejuruteraan Pembuatan, Universiti Teknikal Malaysia Melaka, Hang Tuah Jaya, 76100 Durian Tunggal, Melaka, Malaysia
[2)] Fakulti Kejuruteraan Teknologi Mekanikal dan Pembuatan, Universiti Teknikal Malaysia Melaka, Teknologi Kampus, 75450, Hang Tuah Jaya, Melaka, Malaysia

[*]Corresponding e-mail: fatimah.abd@mara.gov.my

Keywords: Ergonomic; vibration, KTM Komuter Berhad

ABSTRACT – The purpose of this study is to assess the exposure of the whole body vibration (WBV) to the passenger. In this experiment, three factors, namely the route, the location of the tri-axial pad, and the WBV value as the response were studied. Results showed that WBV value at gangway area in Experiment 5 gives the higher values than others. Result of this study can provide awareness to the passengers in order to have less effect of WBV when travelling using KTM Komuter Berhad.

1. INTRODUCTION

Vibration, as defined in Oxford Dictionaries, is "an instance of vibrating or a person's emotional state, the atmosphere of a place, the associations of an object, as communicated to and felt by others". In physic, vibration is defined as an "oscillation of the parts of a fluid or an elastic solid whose equilibrium has been disturbed or of an electromagnetic wave". In ergonomic environment meaning, vibration is defined as any regular movement a body makes about a fixed point [1]. In the industry environment, ergonomics seeks to prevent injuries and to improve comfort while on the job, whereas ergonomic risk factors will impose a biomechanical stress on worker. There are also examples about vibration studies in scope of transportation for an ergonomic attempt such as two-wheeler riders, coach bus, car, truck, and also for railway. Fast development of technology over the last decade has contributed to the negative effect such as vibration that can affect human health (both physical and mental). Exposure to vibrations is associated with a risk of body injury in the form of vascular disorder, nerve malfunction, and effects on the musculoskeletal system [2]. From the vibration produced in the train coach, it will greatly cause a significant amount of discomfort among the passengers. However, vibrations are commonly felt in the train coaches but rarely noticed by the passengers and thus they neglected its implications to them. This research focuses only on the WBV when travelling using train. WBV can be defined as vibration that occur when a greater part of the body weight is supported on a vibrating surface. WBV principally occurs in vehicles and wheeled working machines. Public transport also belongs to the category vehicles that contribute to the ergonomic value; so, it should be taken into account if users want a comfortable ride. One of the daily challenges face by public transportation sector is WBV activities while riding train along passengers' journey. Therefore, it is important to the users to have ergonomics knowledge in making decision which place to stand or to sit during their journey.

2. METHODOLOGY

This study focuses on the WBV inside KTM Komuter women cabin, which placed on three locations of the floor train; near the exit door, under the passenger seat and gangway (as showed in Figure 1) when travelling along 18 stations from Tampin to KL Sentral and return from KL Sentral to Tampin using different track routes. From authors' observation, these three places became are the focus when passengers boarded the train. For every six station, the data recorded were stopped and recontinued until it reached the destination. The aim of this study is to investigate and analyze the WBV value in order to ascertain that it meets the standard of International Standard ISO 2631-1:1997 (as showed in Table 1) and to suggest improvements of good vibration environment to enhance passengers' experience.

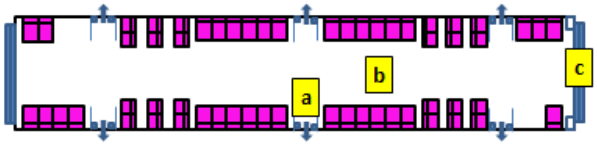

Figure 1 Dytran Model 5313A Tri-Axial IEPE location of seat pad accelerometer at train floor used in this study. (a=at seat, b=at door and c=at gangway).

Table 1 International Standard ISO 2631-1:1997.

RMS acceleration (m/s^2)	Mental reaction of a person
Less than 0.315	Not uncomfortable
0.315 to 0.63	A little uncomfortable
0.5 to 1.0	Fairly uncomfortable
0.8 to 1.6	Uncomfortable
1.25 to 2.5	Very uncomfortable
Greater than 2.0	Extremely uncomfortable

The Dytran Model 5313A was used as a tri-axial Integrated Electronics Piezo Electric (IEPE) seat pad accelerometer for this study. This seat pad accelerometer, which is made of an integral ten (10) foot

cable and terminating to BNC (Bayonet Neil-Concelman) plug, was connected directly to a 4-Channel VI-400PRO human vibration meter (HVM) to record the vibration measurement value. This system was furnished with anti-liasing filters and has International Standard ISO 2631-1:1997 weighting filters. Vibrations were measured in three translational directions: x-axis (longitudinal), y-axis (transverse), and z-axis (vertical). As for the post processing and further analysis, these data were downloaded to a personel computer and dedicated MATLAB-based software was used to enable reading of large waveform audio (WAV) files. There are four values of measures that can be determined using this instrument: acceleration, peak acceleration, crest factor (ratio of peak to average acceleration), and vibration dose value (VDV). This study focuses on root mean square (RMS). WBV measurement explored by the passenger was done 6 times at different train trips areas with a different track as shown in Table 2.

Table 2 Locations of measurement.

Experiment	Location
1	From Tampin to Tiroi
2	From Tiroi to Kajang
3	From Kajang to KL Sentral
4	From KL Sentral to Kajang
5	From Kajang to Tiroi
6	From Tiroi to Tampin

3. RESULTS AND DISCUSSION

Figure 2 results of exposures of vibration between three pad acceleration locations and the experiment area. The highest vibration magnitude computed from the weighted acceleration history of the train floor was obtained as 2.2182 m/s^2 and in the z-direction at the gangway area in the Experiment 5, which travel from Kajang to Tiroi. This value shows that it is extremely uncomfortable for the passenger according to ISO 2631 (in Table 1) when they have to stand around the gangway area. Tracks for the train need to be made maintenance such as grinding the track to get a smooth track surface, so that it can reduce high vibration value along journey at Experiment 5 that affect to the passenger inside the train cabin. Meanwhile, the low value of RMS is at floor near the exit door in x-axis for the journey of KL Sentral to Kajang in the Experiment 4 with the value of 0.5352 m/s^2. By referring Table 1, this low value still gives fairly uncomfortable feeling to the passenger because as mentioned in the introduction, WBV principally occurs in vehicles and wheeled working machines. So, it relates with the fairly uncomfortable result of WBV value for this experiment.

Low level of vibration is an important element for commercialization of public transport because it affects passengers' comfort and satisfaction. Vibration control is an important consideration in train as the constant motion of parts while the train is moving because there will be possible damage to the structural frame or components. The suggestion to using foam tapes can prevent parts such as aircond units, fans, interior panels, floor from touching or rattling during train movement can reduce the vibration value from inside train. The reduction of train track at ground can be done by adding some elastic element such rail pads and sleeper pads. Another suggestion is to put rail vibration absorber to reduce the measurement of vibration along the track.

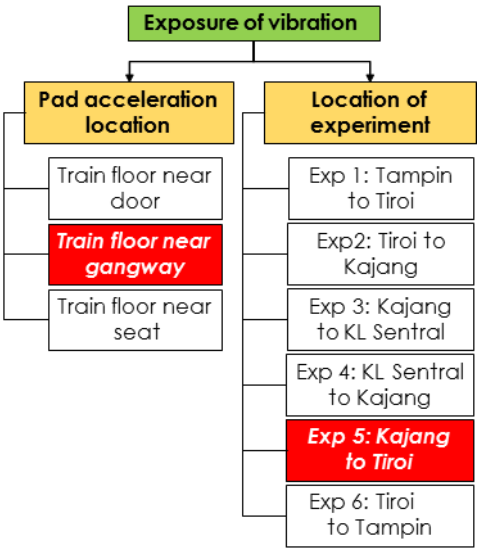

Figure 2 Case study results on exposure of vibration.

4. CONCLUSION

Passengers are advised not to stand within the gangway area because the measurement vibration is high in that floor area. Passengers are recommended to sit and stand near the sear place where the average results of vibration in that area are lower than another place. In conclusion, different values were recorded based on the sitting or standing position of the passengers when riding train. Further studies are required on specific part that influences vibration that leads to high value of WBV and how to overcome it.

ACKNOWLEDGEMENT

This research was co-funded by University Teknikal Malaysia Melaka, Ministry of Higher Education for MyBrain 15 Programme, KTM Komuter Berhad and Majlis Amanah Rakyat (MARA).

REFERENCES

[1] Kolgiri, S., Hiremath, R., & Bansode, S. (2016). Literature Review on Ergonomics Risk Aspects Association to the Power Loom Industry. *IOSR J. Mech. Civ. Eng. Ver. III*, *13*(1), 2278-1684.

[2] Vihlborg, P., Bryngelsson, L., Lindgren, B., Gunnarsson, L. G., & Graff, P. (2017). Association between vibration exposure and hand-arm vibration symptoms in a Swedish mechanical industry. *International Journal of Industrial Ergonomics*, *62*, 77-81.

Parametric study on absorption coefficient of inhomogeneous double-layer MPP

Ali I. Mosa[1,3], A. Putra[1,2,*], R. Ramlan[1,2], Al-Ameri Esraa[1]

[1)] Fakulti Kejuruteraan Mekanikal, Universiti Teknikal Malaysia Melaka,
Hang Tuah Jaya, 76100 Durian Tunggal, Melaka, Malaysia
[2)] Centre for Advanced Research on Energy, Universiti Teknikal Malaysia Melaka,
Hang Tuah Jaya, 76100 Durian Tunggal, Melaka, Malaysia
[3)] Mechanical Engineering Department, Collage of Engineering, University of Baghdad, Jadriyah - Baghdad, Iraq

[*]Corresponding e-mail: azma.putra@utem.edu.my

Keywords: Sound absorption, inhomogeneous MPP, multi-cavity depth

ABSTRACT – A micro-perforated panel (MPP) has been presented as an alternative absorber to the conventional fibrous and porous absorber. However, it's bandwidth still narrow comparing to porous materials. In this paper a parametric study of applying an inhomogeneous panel pattern on double layer MPP is presented. Using the equivalent circuit method, the mathematical model has been developed. Results shows that applying the inhomogeneous panel pattern to double layer MPP system can produce a wider absorption bandwidth comparing to the homogeneous one. Predicted results are validated through the experiment.

1. INTRODUCTION

As a fibre-free materials, lightweight and have an attractive and aesthetic appearances traditional micro-perforated panel (MPP) sound absorbers are used for building acoustics and interior surfaces because noise control is a major concern that should be considered [1], also they are more robust and suitable for various application [2-4]. MPPs are slim sheets having a set of very small holes, diameters (d < 1 mm) and set in front of rigid wall separated by an air-gap. Through the recent years, the researchers presented several studies to improve the absorption bandwidth of single layer MPP by preform L shape cavity structure [5], used of mechanical impedance plate [6], MPP with membrane cell [7], inhomogeneous perforation [8]. This paper will present a parametric study of applying an inhomogeneous pattern on double layer MPP absorber system and compare with homogeneous one.

2. METHODOLOGY

Figure 1 shows the Schematic diagram of double-layer-inhomogeneous-MPP model, where d_1, d_2, d_3 and d_4 are the hole diameter for each *sub-MPP*, t_1 and t_2, are the panel thickness, D_1 *and* D_2 are the cavity depths of the air gaps. Based on equivalent electrical circuit method the total system impedance can be calculated as [8]

$$Z_1 = Z_{i\mathrm{MPP}_1} + Z_{D_1} \quad (1)$$

$$Z_2 = Z_{i\mathrm{MPP}_2} + Z_{D_2} \quad (2)$$

$$Z_{total} = Z_1 + Z_2 \quad (3)$$

Where $Z_{i\mathrm{MPP}_1}$ and $Z_{i\mathrm{MPP}_2}$ are the impedance of the first panel and the second panel,

Z_{D_1} and Z_{D_2} are the impedance of the first and second cavity which can be calculate by

$$Z_{D_{1,2}} = -j\cot\left(\frac{\omega D_{1,2}}{c}\right) \quad (4)$$

And Z_{total} is the total impedance of the system. Thus, the normal sound absorption coefficient is calculated by

$$\alpha = \frac{4\mathrm{Re}\{Z_{\mathrm{total}}\}}{[1+\mathrm{Re}\{Z_{\mathrm{total}}\}]^2+\mathrm{Im}\{Z_{\mathrm{total}}\}^2} \quad (5)$$

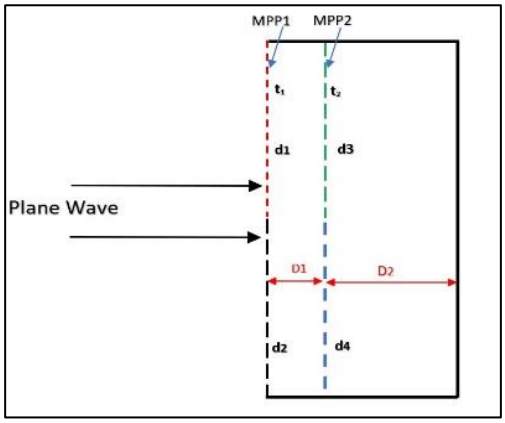

Figure 1 Schematic diagrams of double-layer-inhomogeneous-MPP.

3. RESULTS AND DISCUSSION

Figure 2 shows the comparison of the normal coefficients between conventional single layer (SL-MPP), double layer (DL-MPP) and the presented model (DL-iMPP) connecting in a series arrangement. It clear that wider absorbing bandwidth can be obtained by performing an inhomogeneous pattern for double layer MPP, however the first peak slightly shifts toward high frequency. The structure parameters of the simulated models are listed in Table 1, all thicknesses are set at 1 mm.

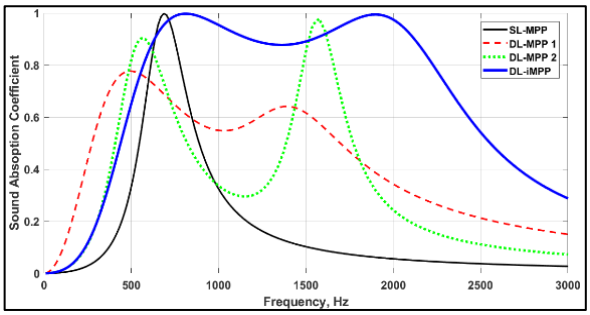

Figure 2. Comparison of absorption coefficients between SL-MPP, DL-MPP and DL-iMPP, cavity depth: D_1 = 20 mm, D_2 = 32 mm.

Table 1 list of Parameters of SL-MPP, DL-MPP and DL-iMPP.

Model	MPP layer 1				MPP layer 2			
	d_1 mm	d_2 mm	p_1 %	p_2 %	d_1 mm	d_2 mm	p_1 %	p_2 %
SL MPP	0.8		0.6					
DL MPP_1	0.3		1		0.3		1	
DL MPP_2	0.8		1.5		0.8		1.5	
DL iMPP	0.8	0.2	0.6	1.5	0.3	0.7	2.5	1

4. EXPERIMENTAL WORK

Figure 3 shows the verifying of the presented (DL-iMPP) model by a comparing the predicted normal coefficient data with experimentally measured data in frequency range from 10 Hz up to 3 kHz. Samples were test in impedance tube in lab. The MPPs are constructed with a two size of hole diameter and ratio with large difference to produce a wide bandwidth of absorption as found in [8-9]. Figure 3a parameters are: 1st layer MPP: t_1 = 1 mm, d_1 = 0.3 mm, d_2 = 0. 6 mm, p_1 = 4.0%, p_2 = 0.6% and 2nd layer MPP: t_2 = 1 mm, d_3 = 0.3 mm, d_4=0.5 mm, p_3=3.5%, p_4 = 1.5%. Figure 3b parameters are: 1st layer MPP: t_1 = 1 mm, d_1 = 0.3 mm, d_2 = 0. 5 mm, p_1 = 0.2%, p_2 = 3.0% and 2nd layer MPP: t_2 = 2 mm, d_3 = 0.5 mm, d_4=0.3 mm, p_3=1.5%, p_4 = 3.5%.

Measured results show a good agreement with the predict results, however the 3rd peak of the predicted curve shows slightly shift in Figure 3(a) and lower value in Figure 3(b).

5. CONCLUSION

In this paper a parametric study of applying an inhomogeneous panel pattern on double layer MPP absorber system model is presented. Mathematical equations are developed based on the equivalent circuit method. Results shows that double layer inhomogeneous MPP model can produce wider absorption bandwidth with than the conventional double layer MPP for the same setting parameters without enlarging the cavity depth. Predicted results are validated through the experiment, which are show a good agreement.

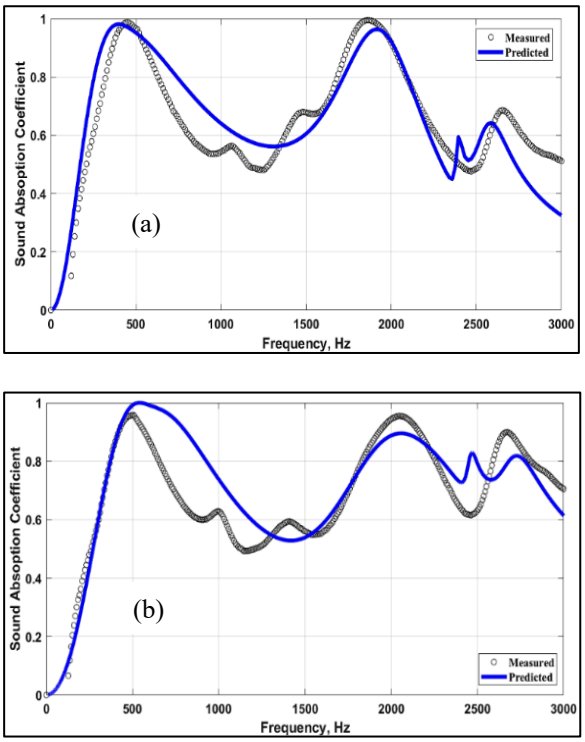

Figure 3 Comparison of normal absorption coefficients between predicted and measured data of DL-iMPP model, cavity depths are D_1 = 20 mm, D_2 = 75 mm.

ACKNOWLEDGEMENT

Part of this project is supported by the Fundamental Research Grant Scheme from Ministry of Higher Education Malaysia. (Grant no.: FRGS/1/2016/TK03/FTK-CARE/F00323).

REFERENCES

[1] Dah-You, M. A. A. (1975). Theory and design of microperforated panel sound-absorbing constructions. *Scientia Sinica*, *18*(1), 55-71.

[2] Ismail, A. Y., Putra, A., & Ayob, M. R. (2011). Application of micro-perforated panel (MPP) in a Vehicle vabin: Overcoming the 'mass-air-mass' resonance. *Hari Penyelidikan FKM 2011,* 46–51, 2011.

[3] Shi, X., & Mak, C. M. (2017). Sound attenuation of a periodic array of micro-perforated tube mufflers. *Applied Acoustics*, *115*, 15-22.

[4] Yu, X., Lau, S. K., Cheng, L., & Cui, F. (2017). A numerical investigation on the sound insulation of ventilation windows. *Applied Acoustics*, *117*, 113-121.

[5] Gai, X. L., Xing, T., Li, X. H., Zhang, B., Wang, F., Cai, Z. N., & Han, Y. (2017). Sound absorption of microperforated panel with L shape division cavity structure. *Applied Acoustics*, *122*, 41-50.

[6] Zhao, X. D., Yu, Y. J., & Wu, Y. J. (2016). Improving low-frequency sound absorption of micro-perforated panel absorbers by using mechanical impedance plate combined with Helmholtz resonators. *Applied Acoustics*, *114*, 92-98.

[7] Gai, X. L., Li, X. H., Zhang, B., Xing, T., Zhao, J. J., & Ma, Z. H. (2016). Experimental study on sound absorption performance of microperforated panel with membrane cell. *Applied Acoustics*, *110*, 241-247.

[8] Mosa, A. I., Putra, A., Ramlan, R., Prasetiyo, I., & Esraa, A. A. (2019). Theoretical model of absorption coefficient of an inhomogeneous MPP absorber with multi-cavity depths. *Applied Acoustics*, *146*, 409-419.

[9] Mosa, A. I., Putra, A., Ramlan, R., Esraa, A., & Halim, Z. (2018). Parametric study on performance of an inhomogeneous MPP absorber. *Proceedings of Mechanical Engineering Research Day 2018*, 303–304.

Study of sound absorption of micro perforated panel with visco-thermal effects

Al-Ameri Esraa[1], A. Putra[1,2,*], Ali I. Mosa[1,3], R.M. Dan[1,2]

[1)] Fakulti Kejuruteraan Mekanikal, Universiti Teknikal Malaysia Melaka,
Hang Tuah Jaya, 76100 Durian Tunggal, Melaka, Malaysia
[2)] Centre for Advanced Research on Energy, Universiti Teknikal Malaysia Melaka,
Hang Tuah Jaya, 76100 Durian Tunggal, Melaka, Malaysia
[3)] Mechanical Engineering Department, Collage of Engineering, University of Baghdad, Jadriyah - Baghdad, Iraq

[*]Corresponding e-mail: azma.putra@utem.edu.my

Keywords: Sound absorption, inhomogeneous MPP, finite element method (FEM)

ABSTRACT – Micro-perforated panel (MPP) absorbers, are recognized as the next group of sound absorbing materials. Most recent presented research used the analytical method to calculate the acoustic performance of the MPP considering the impedance of single hole and then use the porosity to determine the whole impedance. However, this method not effective for panels with inhomogeneous hole perforation. This study presents 3D model to study the sound absorption of inhomogeneous MPP using FEM considering the visco-thermal effects. Results shows that the simulated data does not match with analytical one. Experiment data showed a good agreement with the simulations data.

1. INTRODUCTION

MPPs absorbers without additional fibrous or porous material has been widely used as the next group of sound absorbing materials. MPPs are tiny panels with a mesh of sub-millimetre size holes circulated over its surface and can made from metal, plastic or etc. [1]. MPP has been taken more interest the researchers because simple construction and obvious sound absorption effect and easy for use. The applications of MPP are extensively used in noise control engineering such as Acoustic silencers [2-3], ducted ventilation [4], building acoustic systems [5-6]. However, the total sound absorption bandwidth is still limited [7]. Most of studies used the analytical method to compute the acoustic performance of the MPP by considering the impedance of a single hole and then use the porosity to determine the whole impedance of the panel. However, this method is not effective for panels with inhomogeneous hole size [8]. Thus, whole or half structure of the model should be impalement to study the impedance of non-homogenous panels. This study presents 3D model to study the acoustic performance of single layer inhomogeneous MPP using FEM considering the visco-thermal effects.

2. SIMULATION ANALYSIS

The theoretical normalized acoustic impedance of inhomogeneous MPP model is calculated by implement a 3D visco-thermal model using a finite element method (FEM) based on the linearized Naiver Stokes equations in the frequency domain [8-9]. Figure 1 shows the MPP sample and its symmetry boundaries, it performed inside a cylindrical impedance tube has a length of 30 cm and inner diameter of 3.3 cm.

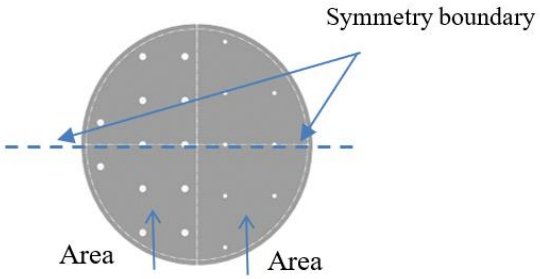

Figure 1 Schematic graph of inhomogeneous MPP with the assumed symmetry boundaries.

The calculated transfer acoustic impedance (Z_{trans}) of the panel by FEM including the visco-thermal effect, which can give by [10].

$$Z_{MPP} = Z_{trans} = \frac{\int P_{in} - \int P_{out}}{\rho c \int v} \quad (1)$$

Where Δp is the pressure drop across the panel, v is the velocity in the perforation hole, ρ density of air. Thus, the normal absorption coefficient α of the model including the visco-thermal effect by FEM can be represented as [10].

$$\alpha = 1 - |R|^2 \quad (2)$$

Where R is the pressure reflection coefficient that gives as

$$R = \frac{\int P_{scat}}{\int P_{inc}} \quad (3)$$

Where P_{scat} is the scattered sound pressure and P_{inc} is incident sound pressure. The calculation was made under ideal air physical properties. While the total impedance calculated by electric circuit method (ECM) is

$$Z_{total} = r + j\omega m + Z_D \quad (4)$$

Where r is $Z_{resistive}$, $m\ is\ Z_{reactive}$, Z_D is impedance of cavity depth.

3. RESULTS AND DISCUSSION

Figure 2. shows the comparison between the imaginary part of the normalized impedance imag (Z_{trans}) calculated by FEM and (ECM) described of the MPP model. Model structure parameters are for area 1 are hole diameter d_1 = 0.9mm, perforation ratio $p_{1=}$ 1.76%, for

area 2 are hole diameter d_2 = 0.5 mm, perforation ratio $p_{2=}$ 0.4 %. Thickness is set to be t=1 mm for the whole panel and cavity depth D=30mm.

Figure 3 shows comparison of absorption coefficient between analytical ECM with the simulated FEM. it can be observed that the results showed un-agreement. These un-agreement are mainly due to the finite geometry effect and to the spatial distribution of the perforations for the numerical case [8].

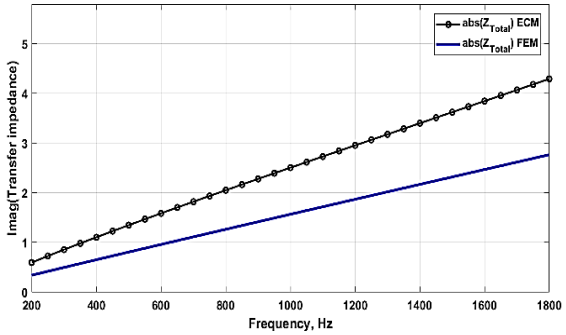

Figure 2. Total impedance comparison between FEM and ECM of a single layer inhomogeneous MPP, cavity depth D= 30 mm.

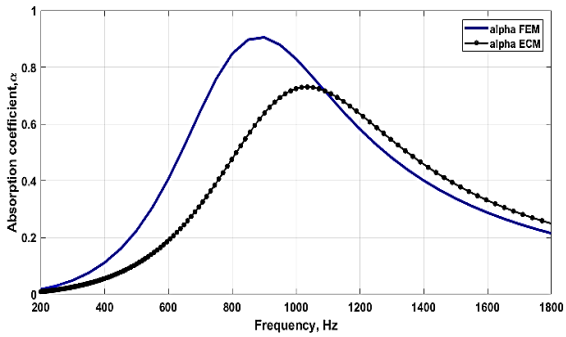

Figure 3. Absorption coefficient comparison between FEM and ECM of single layer inhomogeneous MPP, cavity depth D= 30mm.

4. MODEL VALIDATION

Figure 4 shows the validation of the FEM model with experimentally measured data of normal absorption coefficients. Experiment data were obtained in lab by using of impedance tube according to the standard ISO 10534-2[11] .A good agreement can be observed This lead that the FE model with considering the visco-thermal effect can accurately describe the acoustic performance for the analysed configurations. [8].

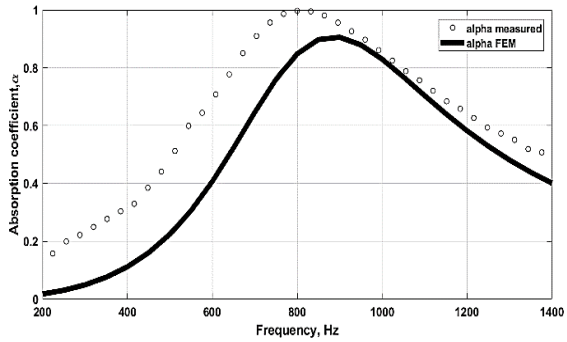

Figure 4. Absorption coefficient comparison between measured data and FEM data, cavity depth D= 30mm.

5. CONCLUSION

In this paper, a 3D FEM model is present in order to study the acoustic properties of inhomogeneous MPPs including the visco-thermal effects. Results show that the absorption performance of MPPs with viscous and thermal is mostly affected and dos not much with the one that obtained by analytical method. The model is experimentally verified and showed a good agreement. This lead that the FE model can accurately describe the acoustic performance for the analysed configurations of inhomogeneous MPPs.

ACKNOWLEDGEMENT

Part of this project is supported by the Fundamental Research Grant Scheme from Ministry of Higher Education Malaysia. (Grant no.: FRGS/1/2016/TK03/FTK-CARE/F00323).

REFERENCES

[1] Dah-You, M. A. A. (1975). Theory and design of microperforated panel sound-absorbing constructions. *Scientia Sinica*, *18*(1), 55-71.

[2] Shi, X., & Mak, C. M. (2017). Sound attenuation of a periodic array of micro-perforated tube mufflers. *Applied Acoustics*, *115*, 15-22.

[3] Yu, X., Cheng, L., & You, X. (2015). Hybrid silencers with micro-perforated panels and internal partitions. *The Journal of the Acoustical Society of America*, *137*(2), 951-962.

[4] Yu, X., Cui, F. S., & Cheng, L. (2016). On the acoustic analysis and optimization of ducted ventilation systems using a sub-structuring approach. *The Journal of the Acoustical Society of America*, *139*(1), 279-289.

[5] Yu, X., Lau, S. K., Cheng, L., & Cui, F. (2017). A numerical investigation on the sound insulation of ventilation windows. *Applied Acoustics*, *117*, 113-121.

[6] Mosa, A. I., Putra, A., Ramlan, R., Prasetiyo, I., & Esraa, A. A. (2019). Theoretical model of absorption coefficient of an inhomogeneous MPP absorber with multi-cavity depths. *Applied Acoustics*, *146*, 409-419.

[7] Li, D., Chang, D., Liu, B., & Tian, J. (2014, October). Improving sound absorption bandwidth of micro-perforated panel by adding porous materials. In *INTER-NOISE and NOISE-CON Congress and Conference Proceedings* (Vol. 249, No. 6, pp. 1877-1882). Institute of Noise Control Engineering.

[8] Carbajo, J., Ramis, J., Godinho, L., Amado-Mendes, P., & Alba, J. (2015). A finite element model of perforated panel absorbers including viscothermal effects. *Applied Acoustics*, *90*, 1-8.

[9] Kampinga, W. R., Wijnant, Y. H., & de Boer, A. (2010). Performance of several viscothermal acoustic finite elements. *Acta acustica united with Acustica*, *96*(1), 115-124.

[10] Li, L., Gang, X., Liu, Y., Zhang, X., & Zhang, F. (2018). Numerical simulations and experiments on thermal viscous power dissipation of perforated plates. *AIP Advances*, *8*(10), 105221.

Development of 3D-printed vibration dynamic absorber

Mohamad Syafiq Hamdan[1], Azma Putra[1,2,*], Mohd Rizal Alkahari[1,2]

[1)] Fakulti Kejuruteraan Mekanikal, Universiti Teknikal Malaysia Melaka,
Hang Tuah Jaya, 76100 Durian Tunggal, Melaka, Malaysia
[2)] Centre for Advanced Research on Energy, Universiti Teknikal Malaysia Melaka,
Hang Tuah Jaya, 76100 Durian Tunggal, Melaka, Malaysia

[*]Corresponding e-mail: azma.putra@utem.edu.my

Keywords: 3D printer; vibration absorber; ABS plastic

ABSTRACT – Vibration of a system can be reduced by using a dynamic vibration absorber. In this study, a vibration absorber is fabricated using using 3D printer machine technology from Acrylonitrile Butadiene Styrene (ABS). The effectiveness of the vibration absorber is tested on a cantilever beam and it is found to successfully reduce the amplitude of the first mode of the beam.

1. INTRODUCTION

A a dynamic vibration absorber is a combination of spring-mass system, where its natural frequency is tuned to the vibration frequency of the host structure [1]. The absorber can therefore be of any form, such as lumped system of mass-spring-damper like those installed at the Taipei 101 building in Taiwan and at Millennium bridge in London, or a continuous system such as the Stockbridge damper.

The most recent research is a study to create vibration absorber using the metamaterial. Metamaterial is a material engineered to have a property with combinations of multiple elements fashioned from composite materials such as plastics or metals.

Lee et al. [2] proposed a vibro-acoustic metamaterial for suppressing longitudinal vibration waves transmitted between two mechanical parts. The absorber is found to effectively reduce vibration in extremely low frequency range of longitudinal vibration.

He et al. [3] designed structural vibration suppression in laminate acoustic metamaterials which is composed of carbon-fiber-reinforced polymer (CFRP) and periodic array of mass-spring-damper subsystems. By integrating these two parallel orthotropic laminates, the stopband becomes wider compared to that of a conventional vibration absorber. Similar study was also conducted by Yang et al. [4], where meta-structure beam is attached with multiple absorbers.

Nowadays, 3D printer machine technology becomes increasingly popular because its flexibility in printing any shape of structure into three dimensions [5]. In this study, the 3D print is used to fabricate a single structure of vibration absorber that able to reduce the vibration amplitude of a targeted system.

2. METHODOLOGY

2.1 Design and Fabrication of Vibration Absorber

The vibration absorber for this project was designed by using Solidwork software. It was designed where part of the vibration absorber will have spring like properties and another part will act as the inertial mass. The model of vibration absorber in this study is as shown in Figure 1.

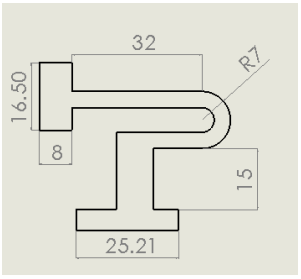

Figure 1 Proposed model of vibration absorber (the dimensions are in mm unit).

The model was then transferred to ANSYS software to calculate the natural frequency of the absorber. The natural frequency of the vibration absorber must in the range of 100 Hz to 200Hz in order to satisfy the requirement for the testing in the lab. The natural frequency of the vibration absorber in Figure 1 is 144 Hz.

The model was then fabricated using 3D printer machine, i.e. Flash Print method. The product is shown in Figure 2.

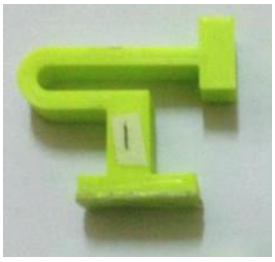

Figure 2 The 3D print product of the designed vibration absorber.

2.2 Experiment

The fabricated vibration absorber was then tested on a cantilever beam model to observe its efficiency in reducing the vibration amplitude of the beam. The experimental setup can be referred in Figure 2. However, prior to this test, the absorber was first installed on the vibration shaker to measure its real natural frequency. The length of the beam was then adjusted, so that its first mode of vibration matches with the natural frequency of the absorber.

The vibration was measured using 'tear drop' accelerometer located off the midspan of the beam. The absorber was attached at distance 7 cm from the free-end

of the beam. One and two absorbers were used and the effect is discussed.

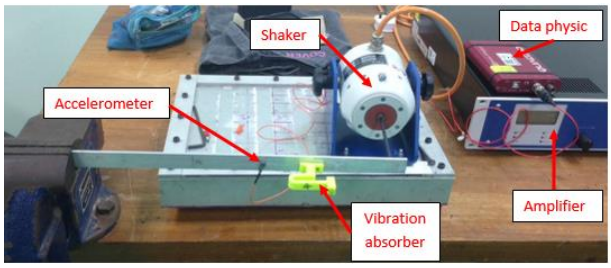

Figure 2 Experimental set up for vibration absorber testing.

3. RESULTS AND DISCUSSION

3.1 Stress Analysis

The stress analysis has been done using ANSYS software to determine the strength and the weakest point of the vibration absorber. The result is shown in Figure 3.

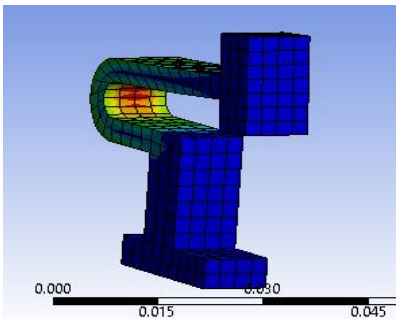

Figure 3 Stress analysis on the vibration absorber.

From Figure 3, the red colour section showed the weakest point on the vibration absorber where stress amplitude is the greatest. During vibration, this curved section in the absorber has the greatest deflection due to its lowest dynamic stiffness.

3.2 Dynamic Test Results

Figure 4 and Figure 5 show the measured vibration amplitude without and with the vibration absorber, for single and two absorbers, respectively. The beam can be seen to have the natural frequency of 144 Hz, which has been set to be the same as the natural frequency of the absorber. From Figure 4, it can be seen that the vibration amplitude of the beam can be reduced significantly at 144 Hz.

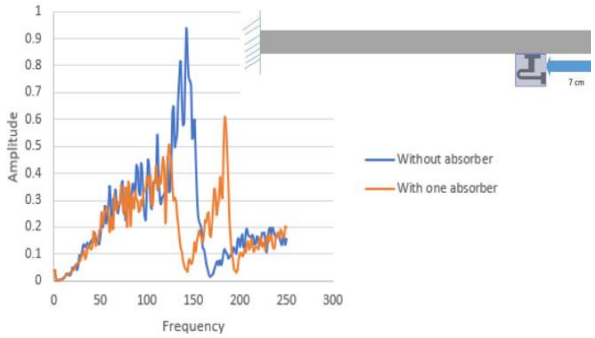

Figure 4 The measured vibration amplitude of the beam with one absorber.

Two resonant frequencies at 130 Hz and 180 Hz can be observed as the consequences of the dynamics of two-degree-of freedom system due to the presence of the absorber on the beam.

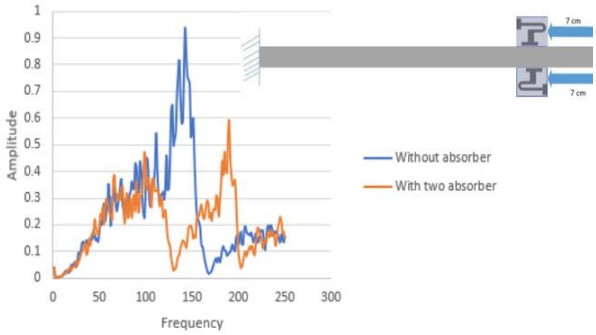

Figure 4 The measured vibration amplitude of the beam with two absorbers.

From Figure 5, adding parallel absorber (on the other side of the beam) can be seen to improve the bandwidth of reduction where the first resonant peak is now reduced at aroun 120 Hz and the second peak has a lower amplitude.

4. CONCLUSION

Vibration absorber produced from 3D print has been successfully fabricated. The dynamic test on a cantilever beam reveals that the product can act as the dynamic absorber to reduce the vibration of the host structure.

It is interesting for the future study to observe the effect of multiple absorbers with different type of arrangement in the structure. The life span of this kind of 3D print product is also of interest to know the reliability of the absorber in practice.

ACKNOWLEDGMENT

Part of this project is supported by Universiti Teknikal Malaysia Melaka with research grant no. JURNAL/2018/FKM/Q00010.

REFERENCES

[1] Rao, S. S., & Yap, F. F. (2011). *Mechanical vibrations* (Vol. 4). Upper Saddle River: Prentice hall.

[2] Lee, S., Ahn, C. H., & Lee, J. W. (2018). Vibro-acoustic metamaterial for longitudinal vibration suppression in a low frequency range. *International Journal of Mechanical Sciences*, *144*, 223-234.

[3] He, Z. C., Xiao, X., & Li, E. (2017). Design for structural vibration suppression in laminate acoustic metamaterials. *Composites Part B: Engineering*, *131*, 237-252.

[4] Yang, W., Seong, Y., Jeong, S., & Park, J. (2018). Vibration reduction using meta-structures composed of tuned dynamic absorbers employing mass impacts. *Composite Structures*, *183*, 216-220.

[5] Habeeb, H. A., Alkahari, M. R., Ramli, F. R., Hasan, R., & Maidin, S. (2016). Strength and porosity of additively manufactured PLA using a low cost 3D printing. *Proceedings of Mechanical Engineering Research Day*, *2016*, 69-70.

Vibration analysis for angular misalignment on spur and helical gear

K. Amri Tofrowaih[1,2,*], Abdul Munir Hidayat Syah Lubis[1,2], Mohd Anas Amir[1]

[1)] Fakulti Teknologi Kejuruteraan Mekanikal dan Pembuatan, Universiti Teknikal Malaysia Melaka, Hang Tuah Jaya, 76100 Durian Tunggal, Melaka, Malaysia
[2)] Centre for Advanced Research on Energy, Universiti Teknikal Malaysia Melaka, Hang Tuah Jaya, 76100 Durian Tunggal, Melaka, Malaysia

[*]Corresponding e-mail: khairul.amri@utem.edu.my

Keywords: Condition-based maintenance (CBM); misalignment gear; spectral analysis

ABSTRACT – Vibration of angular misaligned spur and helical gear was analyzed by using spectral analysis in this work to determine the effect of load on misaligned spur and helical gear. Vibration signal for angular misalignment 0˚, 30˚, and -30˚ with different load of 0 Nm, 1.7 Nm, and 3.4 Nm is recorded. Angular misalignment could be observed clearly at 2X RPM at acceleration sensor 1 position. Vibration reading also increases as the load from Brake & Load unit is connected to the output shaft of the gear train system.

1. INTRODUCTION

Common rotating machinery issues such as unbalance, looseness, misalignment, bent shaft and bearing defects can cause undesirable vibration to the overall mechanical system. Gear misalignment could affect its nearby bearing to high wear rate earlier than it should by giving more fatigue stress due to higher concentrated load than design specification [1]. Condition-based maintenance (CBM) is a common technique to assess and monitor condition of pump, gearbox or other machinery components without physically assess it. This method allows maintenance work to be scheduled and provide time for the action to be taken before a failure occurs [2]. Aherwar & Khalid [3] listed four main vibration analysis technique for diagnostic of gearbox namely Time Domain Analysis, Frequency Domain Analysis which includes Spectral Analysis, Order Analysis, and Time Synchronous Averaging. On the other hand, Sait & Eldeen [4] categorized vibration-based analysis into two main different processing groups namely Time-Statistical Analysis and Time-Frequency Analysis. Dalpiaz [5] in his work observed that spectral (or frequency) analysis is the most frequently used vibration analysis method for condition-based monitoring in gear train systems. It is also recommended for detection and basic diagnosis of errors in simple rotating equipment.

2. METHODOLOGY

Vibration signal of a normal condition gear without misalignment, and angular misaligned gear 30˚, and -30˚ which obtained through asymmetrical adjustment of the bearing covers are measured for two types of gear namely spur gear and helical gear. Technical specification of the gears is as shown in Table 1. Vibration is measured by using two acceleration sensors located horizontally at two ends of gear casing to observe vibration tendency. Position of accelerometer 1 is at the right back of the gear casing which near to an induction motor. The 0.37 kW motor provides rotation to the simple gear train via coupling at the shaft at 1800 RPM speed. Brake and Load unit located on the right box as shown in Figure 1 comprises of control unit, electric display and magnetic particle brake. The unit purpose is to simulate the addition of load into the gear system which are 1.7 Nm and 3.4 Nm. There is no adjacent machine operate next to this experiment that would affect vibration level through foundation or structure [1]. Spectral analysis method is used to analyse the vibration signal. Data from spectral analysis is extracted and summarized to a line graph as shown in Figure 2.

Table 1 Technical specification for gear.

Dimension (L x W x H)	260 x 210 x 180 mm
Weight	20kg
Basic profile	DIN 867
Modulus	2
Pressure angle	20˚
Helix angle	10˚
Transmission ratio	i = 3
Centre distance	101.543 mm
Pitch diameter of large gear	151 mm
Pitch diameter of small gear	51 mm

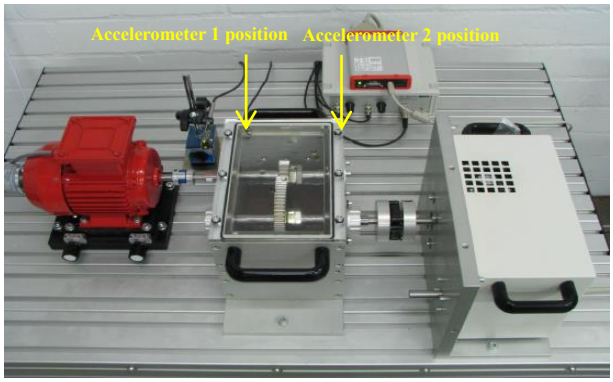

Figure 1 Experimental setup for vibration on gearbox.

The benefit of frequency spectrum analyser in a machine monitoring environment is its capability to display vibration data in the frequency domain as a spectrum. The frequency spectrum shows root mean square (rms) velocity and frequency reading in vertical and horizontal axis respectively. Bruel and Kjaer suggested that a vibration severity is best indicated by velocity-rms for velocity in the range of 10 to 1000 Hz [6]. Moreover, velocity-rms is the standard unit of

vibration measurement as recommended by International Standards Organization (ISO) because it best represents the energy content in a vibration signal, [7]. The ratio of the gear is 1:3 small gear to large gear number of teeth difference. The frequency of 10Hz and 30Hz was derived from the gear ratio considering the induction motor speed equals to 30 Hz. Meanwhile, 60Hz from the graph is 2X RPM of the gear. Engagement frequency or Gear Mesh Frequency (GMF) is equal to 750 Hz.

3. RESULTS AND DISCUSSION

In overall, vibration signal obtained from accelerometer 2 is larger than the vibration signal obtained from accelerometer 1 for most range of loads, gear types and misalignment setting. This shows that the vibration tendency is towards the side of brake & load unit where the accelerometer 2 is located. The graph at 0˚ angle, accelerometer 1 without load indicates control sample reading where only inertia is acting on the gear for 10 Hz is 0.38 mm/s at spur gear and 0.09 mm/s at helical gear. On the other hand, acceleration sensor position 2 with similar parameter recorded 0.69 and 0.30 mm/s. Addition of 1.7 Nm load to the system increase the vibration reading for instance at frequency of 10 Hz for spur gear at 0˚ misalignment angle at sensor 1 position is 0.75 mm/s of spur gear and for helical gear is 0.10 mm/s. At the 2X RPM, the result from spur gear is 0.15 mm/s and from helical gear is 0.04 mm/s, at the 750 Hz the spur gear is 0.07 mm/s and helical gear is 0.01 mm/s.

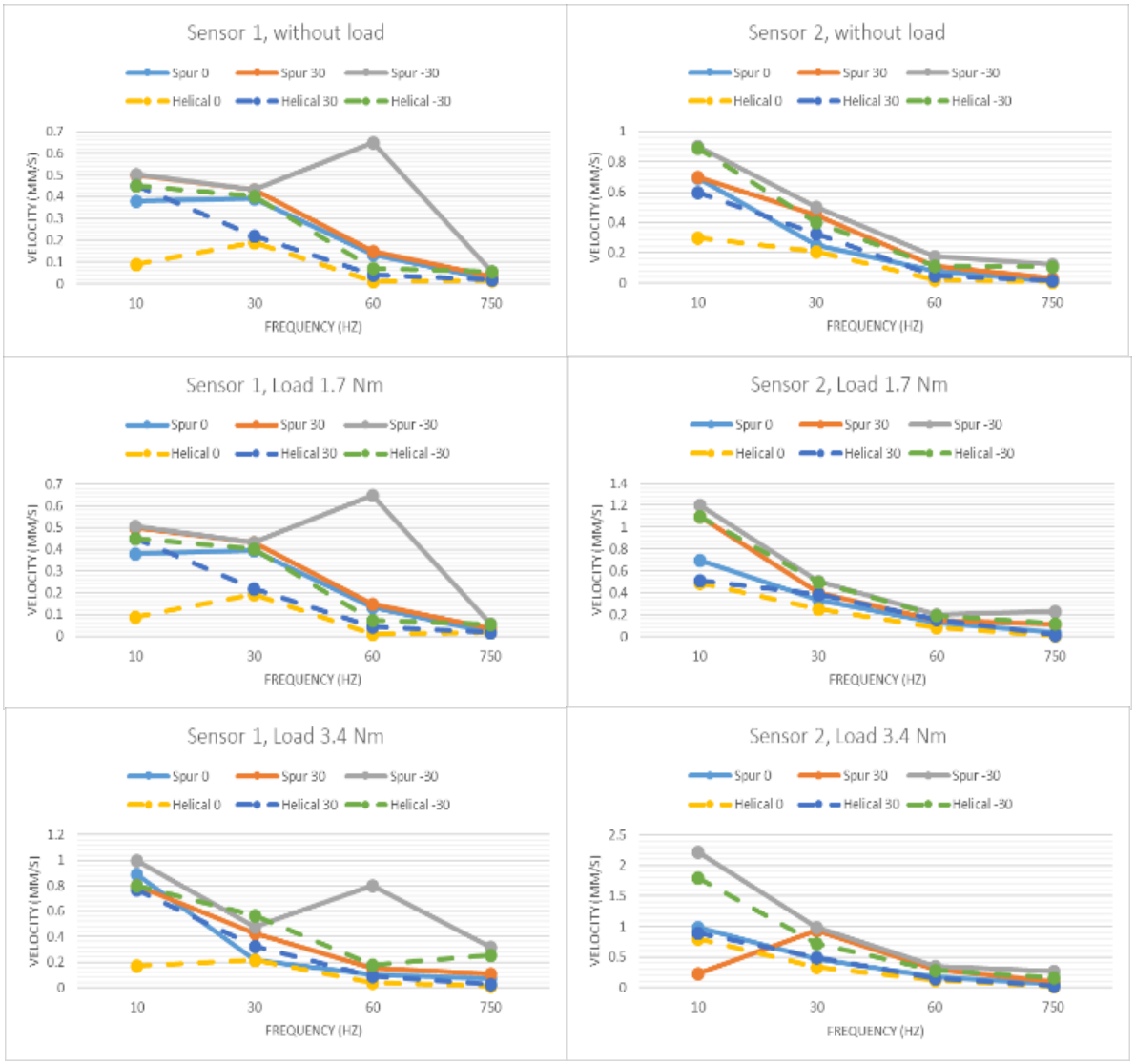

Figure 2 Vibration signals of misaligned spur and helical gear with various load across frequency range.

As the bearing cover is adjusted at 30˚, at acceleration sensor position 1 with frequency of 10 Hz on 3.4 Nm load, the rms velocity reading is 0.89 mm/s for spur gear and 0.17 mm/s for helical gear, whereas at frequency 30 Hz the result is 0.22 mm/s for spur gear and 0.21 mm/s for helical gear was recorded for spur gear and helical gear at frequency 30 Hz with similar load. The value from frequency spectrum of spur gear at 2X RPM is 0.10 mm/s and helical gear is 0.04 mm/s, while the mesh frequency for 30˚ is 0.11 mm/s for spur and 0.03 mm/s for helical gear. However, when the cover is adjusted to -30˚, the spur gear is observed to experience angular misalignment at accelerometer 1 position by the spike of the velocity value at 2X RPM (60Hz). This occurred because load distribution of the gear pair vibration has shifted as suggested in previous study [8]; whereas helical gear is still operating under normal curve pattern. From this single graph, the tolerance of helical

gear towards misalignment is higher. The overall rms velocity decrease with increasing frequency as shown in Figure 2 indicates the vibration energy declines.

4. CONCLUSION

The more load imposed on the gear, higher the vibration level that will affect the gear. Helical gear vibration level is lower than that of spur gear due to helical gear helix angle that smoothen the gear mesh which in turn shows the its higher tolerance towards misalignment than spur gear type.

REFERENCES

[1] J. Mais (2012) Spectrum Analysis: The key features of analyzing spectra, SKF reability system, SKF USA Inc.

[2] Nuawi, M. Z., Khamis, N. K., Zali, Z., Wan Mahmood, W. M. F., Abdullah, S., & Mohd Nopiah, Z. (2013). A study of engine monitoring system using statistical method. *Applied Mechanics and Materials*, *471*, 193–196.

[3] Aherwar, A., & Khalid, S. (2012). Vibration analysis techniques for gearbox diagnostic: A review. *International Journal of Advanced Engineering Technology*, *3*(2), 4–12.

[4] Sait, A. S., & Sharaf-Eldeen, Y. I. (2011). A review of gearbox condition monitoring based on vibration analysis techniques diagnostics and prognostics. In *Rotating Machinery, Structural Health Monitoring, Shock and Vibration, Volume 5* (pp. 307-324). Springer, New York, NY.

[5] Dalpiaz, G., Rivola, A., & Rubini, R. (1998, October). Gear fault monitoring: comparison of vibration analysis techniques. In *3rd International Conference Acoustical and Vibratory Surveillance Methods and Diagnostics Techniques* (pp. 623-632).

[6] Bruel, & Kjaer. (1982). Measuring vibration. Denmark-K Larson and Son.

[7] Scheffer, C., & Girdhar, P. (2004). *Practical machinery vibration analysis and predictive maintenance*. Elsevier.

[8] Houser, D., Harianto, J., & Talbot, D. (2006). Gear mesh misalignment. *Gear Solutions*, 34-43.

3D-printed lattice structure as sound absorber

Muhammad Fakrul Syahid Che Hamid[1], A. Putra[1,2,*], D.H. Kassim[1,2], M.R. Alkahari[1,2]

[1)] Fakulti Kejuruteraan Mekanikal, Universiti Teknikal Malaysia Melaka,
Hang Tuah Jaya, 76100 Durian Tunggal, Melaka, Malaysia
[2)] Centre for Advanced Research on Energy, Universiti Teknikal Malaysia Melaka,
Hang Tuah Jaya, 76100 Durian Tunggal, Melaka, Malaysia

*Corresponding e-mail: azma.putra@utem.edu.my

Keywords: Lattice structures; sound absorber; absorption coefficient

ABSTRACT – Existing sound absorbers, typically consist of fibres and foams. However, it has low life span and poor resistant to damage. This study investigates on the sound absorption characteristics of lattice structure produce by additive manufacturing to improve acoustical characteristics that cannot be fulfilled by typical sound absorber. Sound absorption coefficient (α) measurement were conducted by using impedance tube apparatus according to ISO 10534-2 standard. The effect of thickness, strut diameter of lattice arms and air gap were determined by comparing α for each sample. It is shown that the lattice structures are able to absorb sound mostly above 1 kHz.

1. INTRODUCTION

Noise pollution become more apparent in the process of modernization that cause various harmful effect to people around the world. These situation can be controlled by using sound absorption materials such as fibres and foams [1-5]. However, producing the sound absorber itself brought harmful effect to environment especially foams materials. Most sound absorbers are poor in strength, tend to deteriorate and bulky which are not favourable in lightweight application such as transportation industries and aerospace [6]. Ensuring repeatability in quality is difficult and sometimes increase production time and cost [7-8]. Additive manufacturing enable manufacturers to skip complex process on the new product development and also produce closer characteristics to stochastic foams standard. It became reliable to industrial application due to the simple processing to produce a complex and reliable product [9]. The objective of this paper is to study body centre cubic (BCC) lattice design structure sound absorption coefficient characteristics. Apart from these, the lattice structure and its porosity also considered for making a good absorber.

2. METHODOLOGY

2.1 Lattice Sample

The design of lattice structures was drawn by referring to the BCC type lattice. A single lattice was arranged and stacked to form cylindrical shape to fit in the impedance tube. Sample thickness were varied to 15 mm, 20 mm and 40 mm as shown in Figure 1. The strut diameter of the lattice arms was varied to 1.4 mm, 1.6 mm and 1.8 mm as shown in Figure 2.

Samples were printed by CubePro3D printer using fused deposition method. The material use for the printing is Acrylonitrile Butadiene Styrene (ABS) plastic as it is known with flexibility, smoothness and more reliable when subjected to external impacts compared to other raw materials.

Figure 1 Example of the lattice structure with height of 15 mm and 20 mm.

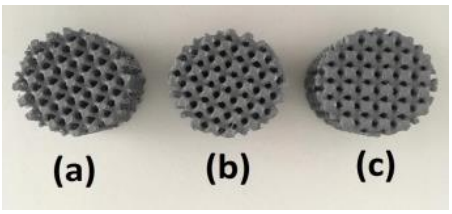

Figure 2 Different strut diameter for lattice (a) 1.4 mm, (b) 1.6 mm and (c) 1.8 mm.

2.2 Experimental Setup

Sound absorption coefficient characteristics were measured using impedance tube with diameter of 33.33 mm with a rigid backing. All measurements were performed using two microphone method following the ISO 10534-2 standard.

3. RESULTS AND DISCUSSION

The data for the sound absorption characteristics of the lattice structures from the experiment were analysed based on the effect of the thickness, strut diameter of lattice structure and application of air gap behind the samples.

3.1 Effect of Thickness

The effect of lattice thickness is shown in Figure 3. However, the peak of α barely reach 0.5 thus a more consideration need to be taken for this parameter. Thicker sample increase peak of α and shift it to the lower frequency. Thicker sample increase flow resistance in the sample and the sound energy dissipation.

3.2 Effect of Strut Diameter

For the effect of strut diameter, the peak of α increase as the strut diameter increase as shown in Figure 4. The samples that have a greater diameter have the higher amplitude of absorption coefficient compared to other sample. The peak value of α is about 0.7 between

tested frequency which is around 1.5 kHz to 2 kHz.

A bigger strut diameter reduce the opening on top of the sample (as seen on Figure 2). A smaller holes produce higher viscous effect thus assist the acoustic dissipation.

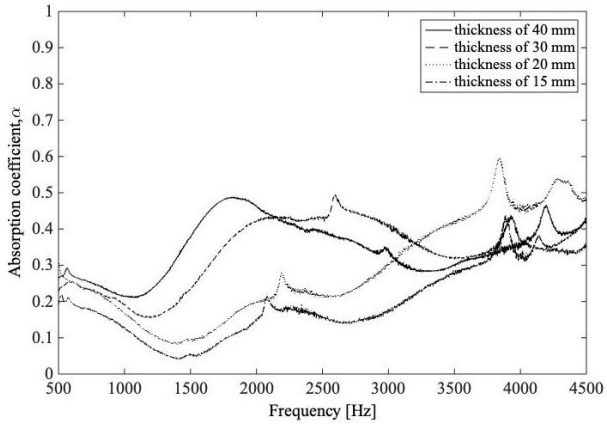

Figure 3 Comparison of lattice structures with different thickness.

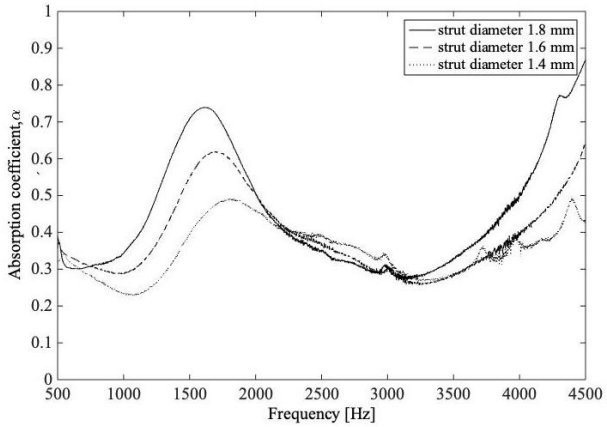

Figure 4 Comparison of lattice structures with different strut diameter.

3.3 Effect of Air Gap

Figure 5 shows with the increasing depth of air gap shift α to lower frequency without much change in its peak. Mass spring resonance created by the presence of air gap and thus peak of α occur when the stiffness of the air gap cancels the mass of the holes in the sample. The presence of air gap layer can be a good alternative technique in order to improve the sound absorption coefficients. However, in dusty environment, unprotected and lowly maintain sound absorber promote the accumulation of dust inside the air gap.

4. CONCLUSION

The performance of lattice structure has been studied and presented in this paper. Based on the result on this experiment, the lattice structures can be suggested to be the next possible sound absorber.

ACKNOWLEDGMENT

Part of this project is supported by Universiti Teknikal Malaysia Melaka with research grant no. JURNAL/2018/FKM/Q00010.

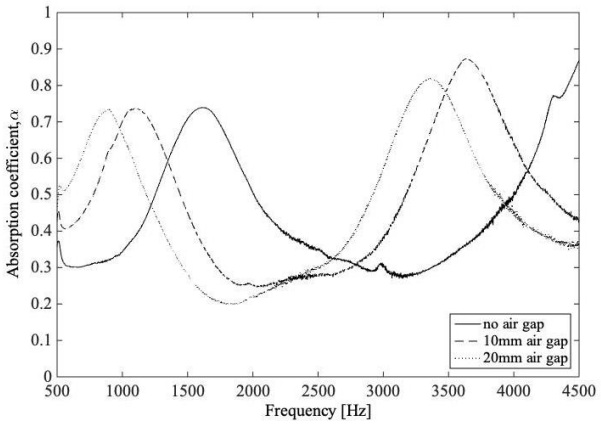

Figure 5 Comparison of lattice structure with the presence of air gap.

REFERENCES

[1] Wang, Y., Zhang, L., Daynes, S., Zhang, H., Feih, S., & Wang, M. Y. (2018). Design of graded lattice structure with optimized mesostructures for additive manufacturing. *Materials & Design, 142*, 114-123.

[2] Lim, Z. Y., Putra, A., Nor, M. J. M., & Yaakob, M. Y. (2018). Sound absorption performance of natural kenaf fibres. *Applied Acoustics, 130*, 107-114.

[3] Ismail, L., Ghazali, M. I., Mahzan, S., & Zaidi, A. M. A. (2010). Sound absorption of Arenga Pinnata natural fiber. *World Academy of Science, Engineering and Technology, 67*, 804-806.

[4] Paşayev, N., Kocatepe, S., & Maraş, N. (2019). Investigation of sound absorption properties of nonwoven webs produced from chicken feather fibers. *Journal of Industrial Textiles*, *48*(10), 1616-1635.

[5] Lu, T. J., Hess, A., & Ashby, M. F. (1999). Sound absorption in metallic foams. *Journal of Applied Physics, 85*(11), 7528-7539.

[6] Fotsing, E. R., Dubourg, A., Ross, A., & Mardjono, J. (2019). Acoustic properties of a periodic micro-structures obtained by additive manufacturing. *Applied Acoustics, 148*, 322-331.

[7] Sauceau, M., Fages, J., Common, A., Nikitine, C., & Rodier, E. (2011). New challenges in polymer foaming: A review of extrusion processes assisted by supercritical carbon dioxide. *Progress in Polymer Science, 36*(6), 749-766.

[8] Jacobs, L. J., Kemmere, M. F., & Keurentjes, J. T. (2008). Sustainable polymer foaming using high pressure carbon dioxide: a review on fundamentals, processes and applications. *Green Chemistry, 10*(7), 731-738.

[9] Petrovic, V., Vicente Haro Gonzalez, J., Jordá Ferrando, O., Delgado Gordillo, J., Ramón Blasco Puchades, J., & Portolés Griñan, L. (2011). Additive layered manufacturing: sectors of industrial application shown through case studies. *International Journal of Production Research, 49*(4), 1061-1079.

Experimental determination of sound absorption coefficient of green materials polymer from different compositions

Farah Liana, Mohamad Ali Ahmad*

Fakulti Kejuruteraan Mekanikal, Universiti Teknologi MARA Shah Alam, 40450 Shah Alam, Selangor, Malaysia

*Corresponding e-mail: mohama9383@uitm.edu.my

Keywords: Green materials; sound absorption coefficient; two-microphone method

ABSTRACT – The usage of synthetic materials has been replaced to natural materials such as banana stem, grass, lemongrass and palm oil leaves to study their sound absorption coefficients. The usage of synthetic materials may lead to numerous problems on human's health and environment. The usage of natural materials may reduce cost and having less health and safety risk while handling and processing. The samples made with diameter 28mm and 100mm and the thickness are 10mm. The sound absorption coefficients of samples were measured according to ASTM E1050-98/ISO 105342-2 two-microphone method. It is evident palm oil leaves material shows high absorption coefficient.

1. INTRODUCTION

Sound can be defined as a physical disturbance in media which has the force and as a transfer medium of sound waves through air, gasses and solids. According to the Minister of Environment Indonesia, noise can be defined as unwanted sound from the business or human activities in the rate and time that can cause human health problems and harm environment [1].

In this study, the most important role to reduce noise is the material of sound absorption [2]. Sound absorptive materials that normally used are fibrous and porous to soften the acoustic environment of a closed volume by reducing the amplitude of the reflected waves. Sound absorber made of synthetic fibre produce significant CO_2 into the atmosphere compared to natural materials [3].

Synthetics porous and fibrous acoustic materials is frequently used in building acoustics also in noise control applications are harmful to human health as well as to the environment [4]. The acoustic panels made from natural fibres are less harmful to human health and eco-friendlier than those made of conventional synthetic fibres [5]. Thus, manufacturers and engineers are inspired to seek alternative materials from natural fibres to replace synthetic fibres due to concern for human health and safety issues. This study is proposed to replace the used of synthetic materials to natural materials by using banana stem, grass, lemongrass and palm oil leaves.

2. METHODOLOGY

The construction flow process of sound absorber was given in Figure 1.

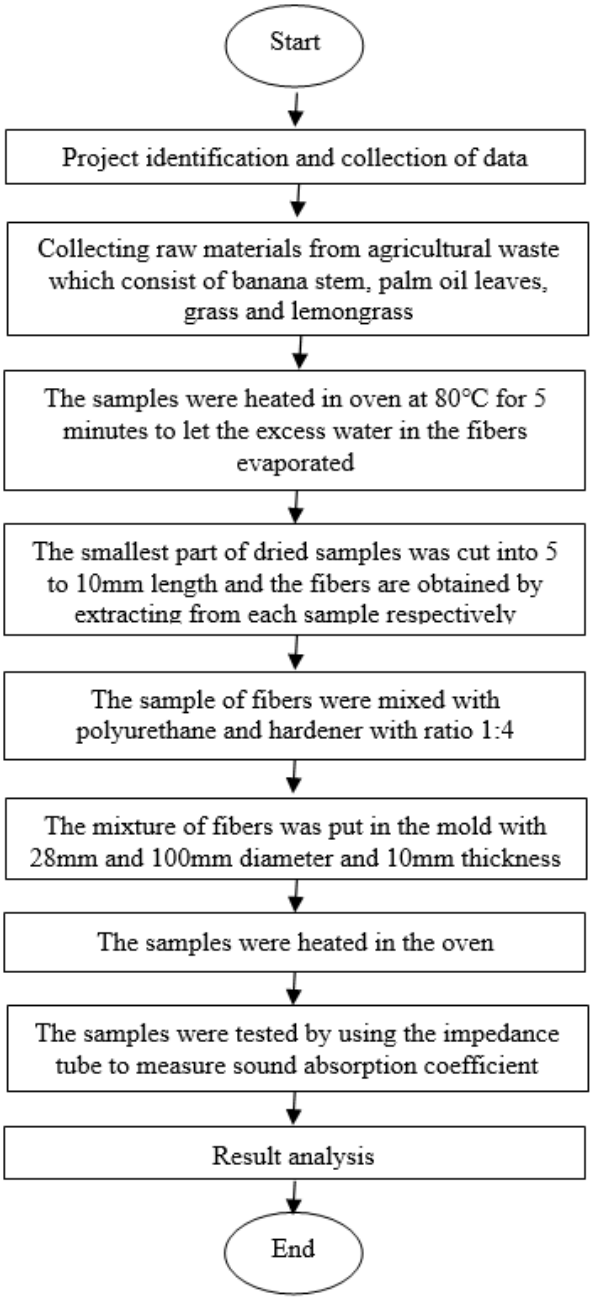

Figure 1 Flow chart of construction process of sound absorber.

3. RESULTS AND DISCUSSION

The measurements were based on a two-microphone (Figure 2) method according to ASTM E1050-98. Figure 3 shows the equipment used in the test and the test set-up. The sample was places at the middle of the impedance tube. Figure 4 shows the variation of sound absorption coefficient against frequency for 4 different samples. It is evident that type of green materials influences the sound absorption coefficients.

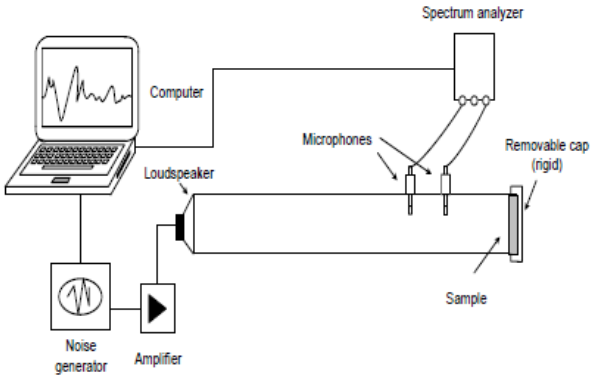

Figure 2 Diagram of the measurement set-ups [5].

Figure 3 Experimental setup and sample specimens.

Table 1 Sound absorption coefficient.

Freq.	Banana stem	Grass	Palm oil leaves	Lemon grass
125	0	0	0	0
250	0.03316	0.03429	0.03075	0.03123
500	0.05282	0.05966	0.04569	0.06323
1000	0.10339	0.14697	0.07852	0.14822
2000	0.42014	0.43586	0.18864	0.45460
4000	0.54971	0.89008	0.95232	0.79980

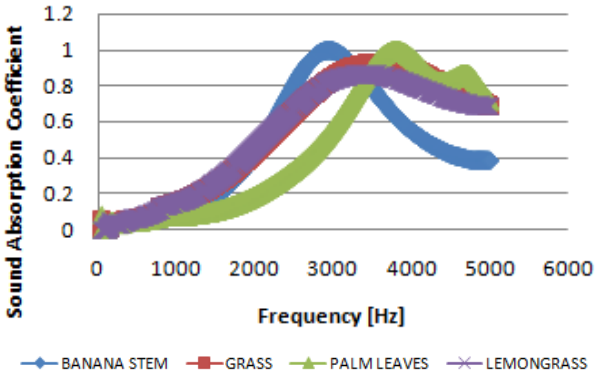

Figure 4 Comparison of sound absorption coefficient of banana stem, grass, palm oil leaves and lemongrass.

All the samples exhibit similar pattern of sound absorption at all frequencies. For all the samples, when the frequency increased, sound absorption coefficient also increased. However, they decreased somewhat at a frequency of 3300 Hz and then increased again. The measured values of the samples show less significant differences on sound absorption coefficient. The sample made of palm leaves shows higher sound absorption coefficients compared to the other materials.

4. CONCLUSIONS

Utilizing green materials as an alternative sound absorbing material has been investigated. The result show that the samples made palm oil leaves have high sound absorption coefficients compared with the other samples. By introducing the sound absorber from green material, the resulting materials show a good potential to be an environmentally products. The new green materials have a good future because they are cheaper and environmentally superior compare to synthetic materials.

REFERENCES

[1] Panggabean, H., Triono, S., & Sukardi. (2017). Acoustic sound absorption material characteristics of fiber using the king banana stem polyurethane and gypsum as matrix. *International Journal of Engineering Research & Technology, 6*(3), 315-322.

[2] Asdrubali, F. (2006). Survey on the acoustical properties of new sustainable materials for noise control. *Proceedings of Euronoise, Tampere*, 1-10.

[3] Jayamani, E., Hamdan, S., & Suid, N. B. (2013). Experimental determination of sound absorption coefficients of four types of Malaysian wood. In *Applied Mechanics and Materials, 315*, 577-581.

[4] Putra, A., Abdullah, Y., Efendy, H., Farid, W. M., Ayob, M. R., & Py, M. S. (2013). Utilizing sugarcane wasted fibers as a sustainable acoustic absorber. *Procedia Engineering, 53*, 632-638.

[5] Fouladi, M. H., Nassir, M. H., Ghassem, M., Shamel, M., Peng, S. Y., Wen, S. Y., ... & Nor, M. J. M. (2013). Utilizing Malaysian natural fibers as sound absorber. In *Modeling and Measurement Methods for Acoustic Waves and for Acoustic Microdevices*, 161-170.

Mobile robotic arm with embedded PID system

Khairuddin Osman[1,2,*], Muhammad Irshad Shaffar Saman[1], Nur Syahirah Eshah Budin Shah[1], Norzahirah Zainuddin[3]

[1)] Fakulti Kejuruteraan Elektronik dan Komputer, Universiti Teknikal Malaysia Melaka, Hang Tuah Jaya, 76100 Durian Tunggal, Melaka, Malaysia
[2)] Centre for Telecommunication Research & Innovation, Universiti Teknikal Malaysia Melaka, Hang Tuah Jaya, 76100 Durian Tunggal, Melaka, Malaysia
[3)] Kolej Komuniti Selandar, Jalan Batang Melaka, 77500 Selandar, Melaka, Malaysia

[*]Corresponding e-mail: khairuddin.osman@utem.edu.my

Keywords: 5-DOF; arduino UNO; PID

ABSTRACT – This paper, the mobile robot has a 5-DOF robotic arm to perform the pick and place task. Besides that, the mobile robot has 4 wheels for mobility. The mobile robot is powered up by 2200mAH Li-PO Battery which can last for an hour. Furthermore, it is built with an Arduino UNO and controlled by Android Smartphone with an app called "JoyStick Controller". Bluetooth is used as a connection between the Arduino and Android Smartphone. The User Interface of the application is designed in a way to allow the user to handle the mobile robot easier. PID controller is used in this project to make the arm movements smooth without barrier and lagging.

1. INTRODUCTION

Nowadays, Robots are significantly increase as robots being immersed into our daily tasks, machines are replacing human especially in industrial sector whereas the automation of process has increase the efficiency while decreasing time consume and human energy. As the technologies getting move advance, the improvement of technologies has inspired whole generation of engineer to push the barriers of technology. The main challenge such as to develop a robotic arm to work the way human arm does.

Human are restricted by physical and mentally limitation whereas robot is invisible. They can work repetitively and way more effectively and efficiency compare to human. They replace human to outperform a duty which human unable to do. Robot do not have soul, they are lifeless. They perform what they are programmed to be and they can work 24/7. They can lift heavy weight and can accurately perform the job with less errors. Robots are widely used in many fields of application including office, industrial automation, military task, hospital operations, security system, dangerous environment, and agriculture [1].

Generally, industrial robotic arm widely used for pick and place task where it is programmed to execute the task to be fast and accurate. From SMT machine to automation, it can work independently or cooperate with human force especially in large scale or heavy weight which human unable to handle. This can greatly reduce the risk factor as well as increase the efficiency of work done [2].

Furthermore, robots are deployed especially in hazardous situation as terrorist bomb threat, land mine patrol and nuclear disaster. They often used to deal with hazardous materials to enhance the human safety especially in hazardous environment such as extremely hot or cold temperature, polluted air, and radioactivity. Human is unable to endure these hazardous environments for a long period [3].

2. METHODOLOGY

Flow chart shows the progression of the research from initial till the end. It is act as a guidance to keep in track on the progress. Whenever there is problem arises, Flow Chart is one of the fastest method to troubleshoot problem. Figure 1 shows the general flowchart of the project.

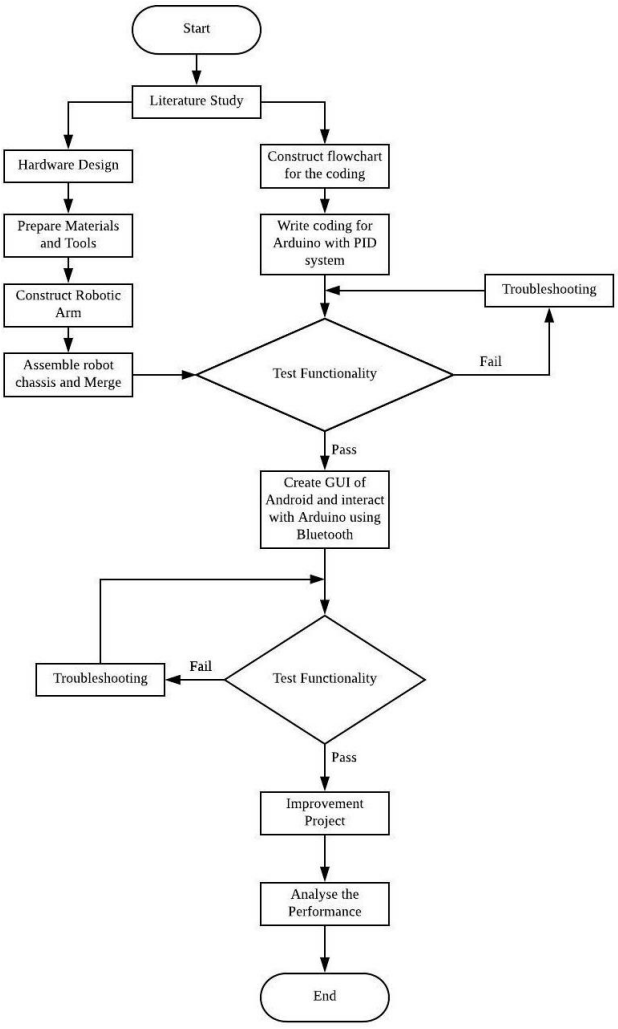

Figure 1 General Flowchart of the project.

Block diagram illustrate the component used in this project. This allows the reader to understand the concept of the project by visualize. In this project, the robot is controlled by android smartphone via Android application, Joystick Controller through Bluetooth Communication. Figure 2 shows the block diagram of the project while the real mobile robot arm with angle for each servo motor is determined based on the Figure 3.

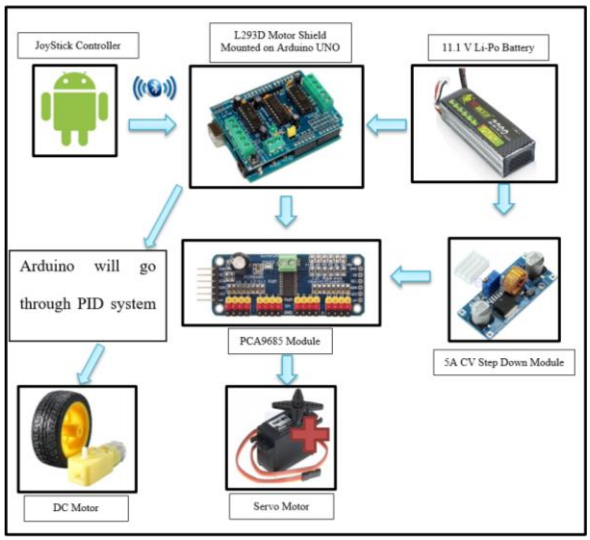

Figure 2 Block diagram of the mobile robot.

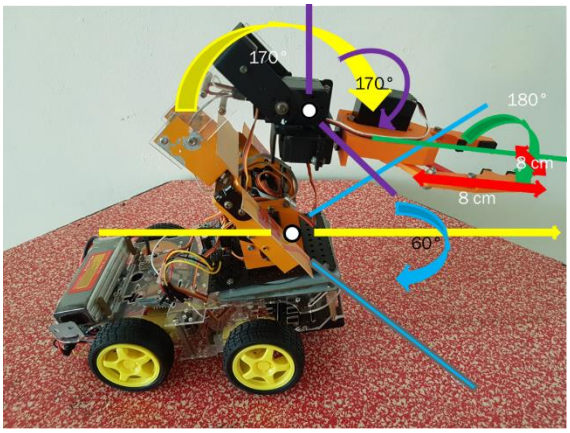

Figure 3 Mobile robot with angle analysis parts.

3. RESULTS AND DISCUSSION

Figure 4 show the graph of distance over time for each speed. It clearly shows that speed 5 took the fastest time to reach the 200m whereas speed 0 took the longest time to reach.

Figure 5 show the comparison between step response with and without the PID controller. The graph without PID controller is in blue colors. There are overshoot occurs in this step response. The steady state error and the settling time are also shown in this graph. Without PID controller the steady state error is 0.33 and the rise time are 1.21 second. The graph in red color is indicate to system with PID controller. In this system there are no overshoot occurs because I can eliminate the overshoot by tune the 3 parameters. The steady state errors are equal to 1 and the rise time is 0.107. The system with PID controller are more appropriate to use because the rise time are 0.107 and make the system steady state error equal to 1. If the rise time decreasing means the input transfer to output are fast. The system with low rise time and steady state error equal to 1 are the stable system. In this project it makes the arm movement with no barrier and lagging.

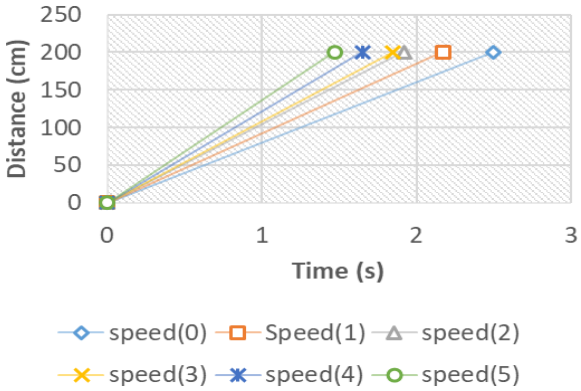

Figure 4 Graph of Distance over Time for each speed.

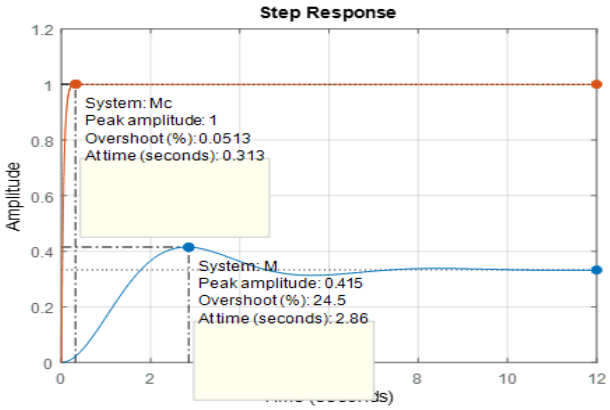

Figure 5 PID controller performance for servo motors.

4. CONCLUSION

The mobile robot with robotic arm can pick and place an object from a destination to another. This has fulfilled the objectives. Besides, the mobile robot is controlled using an Android smartphone. It uses the application called JoyStick Controller to control it, with a polished version of User Interface, it will allow the user to be easier to control the mobile robot as well as the robotic arm. The movement of the robotic arm are smooth and stable with help of PID controller.

ACKNOWLEDGEMENT

The authors would like to thanks Universiti Teknikal Malaysia Melaka (UTeM) under Short Term Research Grant No. PJP/2018/FKEKK(10B)/S01623, Faculty of Electronic and Computer Engineering (FKEKK) and Centre for Telecommunication Research and Innovation (CeTRI) for their support.

REFERENCES

[1] Faravar, A. (2014). *Design, implementation and control of a robotic arm using PIC 16F877A microcontroller* (Doctoral dissertation, Eastern Mediterranean University (EMU)-Doğu Akdeniz Üniversitesi (DAÜ)).

[2] Shah, M. S., & Borole, P. B. (2016, April). Surveillance and rescue robot using Android

smartphone and the Internet. In *2016 International Conference on Communication and Signal Processing (ICCSP)* (pp. 1526-1530).

[3] Kit, W. S., & Venkatratnam, C. (2016, September). Pick and place mobile robot for the disabled through voice commands. In *2016 2nd IEEE International Symposium on Robotics and Manufacturing Automation (ROMA)* (pp. 1-4).

Motion characteristics of a tubular linear switched reluctance actuator (T-LSRA) using phase-to-phase switching algorithm

Chin Kiat Yeo[1], Mariam Md Ghazaly[1,*], Siau Ping Tee[1], Fawwaz Nadzmy[1], Shin Horng Chong[1], Zulkeflee Abdullah[2]

[1)] Center for Robotics and Industrial Automation (CeRIA), Fakulti Kejuruteraan Elektrik,
Universiti Teknikal Malaysia Melaka, Hang Tuah Jaya, 76100 Durian Tunggal, Melaka, Malaysia.
[2)] Fakulti Kejuruteraan Pembuatan, Universiti Teknikal Malaysia Melaka,
Hang Tuah Jaya, 76100 Durian Tunggal, Melaka, Malaysia

[*]Corresponding e-mail: mariam@utem.edu.my

Keywords: Tubular linear switched reluctance actuator; motion characterization; phase-to-phase switching algorithm

ABSTRACT – This paper discussed the motion characteristics of a Tubular Linear Switched Reluctance Actuator (T-LSRA) using phase-to-phase switching algorithm. This paper validates the motion characteristics for both forward and reverse motion. In order to achieve a smooth and fast reciprocating motion, the suitable phase-to-phase switching algorithm corresponding to the mover position was investigated. The mover response time was obtained by reciprocating the mover between 0 mm and 25 mm at maximum rated phase current of 2 A. The tubular LSRA has an overshoot of 33.3 % and requires approximately 0.18 s for the mover to reach the equilibrium position at 5.071 mm.

1. INTRODUCTION

Linear switched reluctance actuator (LSRA) is a fresh type of actuator that has great advantages due to its low cost and simple design construction. However, the key concerns of a SRA are the unwarranted force ripples, vibration and acoustic noise compared to the conventional actuator [1,2]. Hence, the control strategy of the actuator is crucial in order to overcome the drawbacks. Based on studies, several types of controllers have been proposed and applied to switched reluctance actuator (SRA) mechanism; i.e: modified PID control, intelligent control, linearization control and two degrees of freedom control. The PID controller is commonly used in speed and position control applications due to its simplicity, easy tuning and robustness. However, the applied of the conventional PID controller will reduce the positioning performances due to the highly nonlinear characteristics of the SRA. Thus, in order to implement the knowledge of linear controller to a nonlinear system, this system requires to undergo linearization control [3–5]. Hence, Maslan et al. and Ghazaly et al. proposed a new controller to overcome these drawbacks with respect to the precision control by introducing the linearizer unit without any added mechanism [4,5]. Based on the controllers developed by Maslan et al. [4], the proposed PID controller with linearizer unit eliminates the residual vibration caused by applying a linear controller on the LSRA whereby the actuator's characteristic is nonlinear in nature. Subsequently, the maximum steady-state error is approximately four times lower compared to the conventional PID controller. In this research, the phase-to-phase switching algorithm based on Maslan et al. on linear type planar single-sided SRA was implemented in order to evaluate the motion characteristics of the Tubular Linear Switched Reluctance Actuator (T-LSRA) prototype.

2. METHODOLOGY

In this research, the T-LSRA prototype was developed in order to validate the motion characteristics of a T-LSRA by using the phase-to-phase switching algorithm. The linear motion is measured using a linear incremental encoder (RGH24W30D33A, Renishaw) via Micro-box with the interface of MATLAB Simulink Software. Figure 1 shows the full experimental setup in which the assembled T-LSRA prototype. Two polytetrafluoroethylene (PTFE) coated linear bushings are accurately aligned and fitted on both the mover's ends in the direction of motion. This is to ensure the air gap is uniform throughout the actuator and allow low friction sliding surface. Three high current amplifiers (one PBZ60-6.7, Kikusui Electronic Corporation and two TS250-0, Accel Instruments) were used throughout the experimental validation.

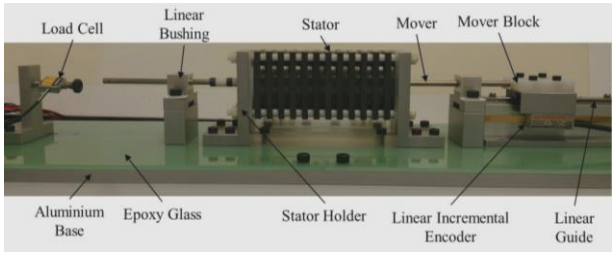

Figure 1 T-LSRA prototype.

In order to achieve smooth and fast reciprocating motion, the suitable phase-to-phase switching algorithm which corresponded to the mover position was investigated. In this paper, forward motion is referred as the mover moves to the left direction and reverse motion is referred as the mover moves to the right direction. The magnetic circuit (magnetic flux) for Phase A at the initial mover position is depicted in Figure 2. When the coils on Phase A are applied with excitation current, magnetic flux is generated and flows from the stator poles with active phase coils to the mover poles and flows back to the stator poles to form a complete cycle of the magnetic circuit. The forward motion and reverse motion sequences in the first pitch for the T-LSRA are shown in Table 1 which was

determined from the open-loop characterization based on the fully aligned mover-to-stator position.

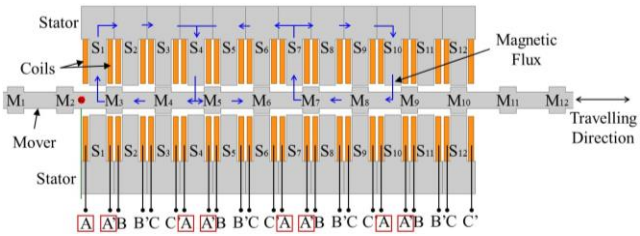

Figure 2 Magnetic circuit for Phase A at initial position.

Table 1 Forward motion sequence in the first pitch.

Position (mm)	Phase	Stator	Mover
0 – 5	AA'	S_1-S_4-S_7-S_{10}	M_3-M_5-M_7-M_9
5 – 10	BB'	S_2-S_5-S_8-S_{11}	M_4-M_6-M_8-M_{10}
10 – 15	CC'	S_3-S_6-S_9-S_{12}	M_5-M_7-M_9-M_{11}

3. RESULTS AND DISCUSSION

The motion characteristics of the T-LSRA was examined through driving characteristics via open-loop experiments. Figure 3 illustrates the block diagram of the open-loop control for the T-LSRA. The open-loop motion characteristic of the mover is evaluated by applying a constant current from 0.9 A to 2 A with 0.1 A increments for 4 s. The excitation phase is depending on the mover position as validated in Table 1.

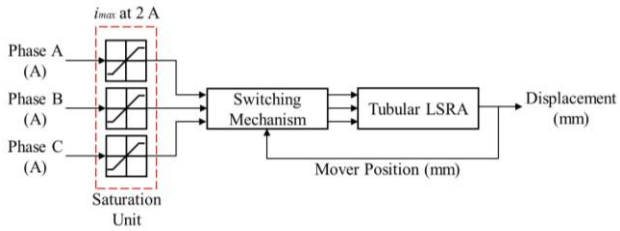

Figure 3 Block diagram of open-loop control for reciprocating motion.

Figure 4(a) depicts the open-loop control of the T-LSRA for one step forward motion at maximum rated phase current of 2 A. Based on the result, the T-LSRA has an overshoot of 33.3 % and requires approximately 0.18 s for the mover to reach the equilibrium position at 5.071 mm instead of 5 mm due to insufficient of energy when the stator and mover poles reach the equilibrium position. To further validate the effectiveness of the phase-to-phase switching algorithm, the open loop control performances for continuous six steps forward and reverse motion at maximum rated phase current of 2 A was evaluated as shown in Figure 4(b).

4. CONCLUSION

In conclusion, the motion characteristics of a T-LSRA using phase-to-phase switching algorithm was successfully verified. The functionality of the developed T-LSRA has been experimentally validated. The T-LSRA motion performances show an overshoot of 33.3 % and require approximately 0.18s for the mover to reach the equilibrium position at 5.071 mm. Through the open-loop reciprocating motion, dynamic responses of the T-LSRA were obtained. The maximum velocity and maximum acceleration that the T-LSRA capable to achieve is approximately 210 mm/s and 8 m/s^2 respectively. Future works include improving T-LSRA control performances toward precision motion.

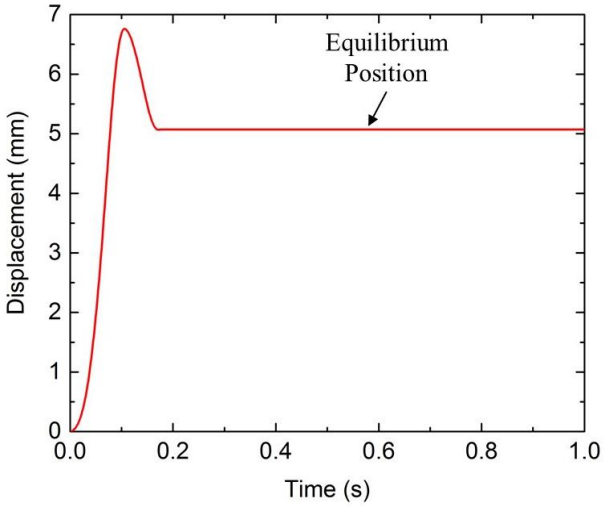

(a)

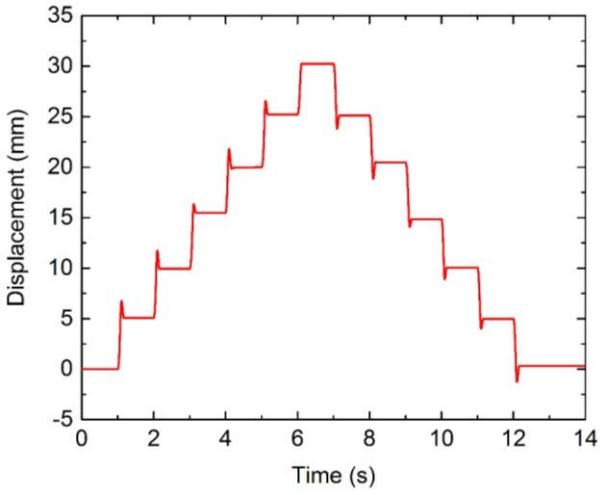

(b)

Figure 4 T-LSRA motion characterization. (a) Open-loop control for one step response and (b) open-loop control for continuous six steps forward motion and reverse motion.

ACKNOWLEDGEMENT

The authors wish to express their gratitude to Motion Control Research Laboratory (MCon Lab), Center for Robotics and Industrial Automation (CeRIA) and Universiti Teknikal Malaysia Melaka (UTeM) for supporting the research and publication. This research is supported by Universiti Teknikal Malaysia Melaka grant no. JURNAL/2018/FKE/Q00006, Center for Robotics and Industrial Automation (CeRIA) and Center for Research and Innovation Management (CRIM).

REFERENCES

[1] Pestana, L. M., Calado, M. R., & Mariano, S. (2016). Experimental force characterization of linear switched reluctance machine. *IEEE 16th International Conference on Environment and Electrical Engineering (EEEIC 2016).* 2016, 1-4.

[2] Yeo, C. K., Ghazaly, M. M., Chong, S. H. & Jamaludin, I. W. (2018). Design optimization of a three phase tubular linear switched reluctance actuator. *ARPN Journal of Engineering and Applied Sciences*, 13(5), 1600–1607.

[3] Gao, X., Wang, X., Li, Z., & Zhou, Y. (2015). A review of torque ripple control strategies of switched reluctance motor. *International Journal of Control Automation*, 8(4), 103-116.

[4] Maslan, M. N., Kokumai, H., & Sato, K. (2017). Development and precise positioning control of a thin and compact linear switched reluctance motor. *Precision. Engineering*, 48, 1-14.

[5] Ghazaly, M. M., & Sato K. (2012). Basic characteristics of a multilayer thin electrostatic actuator supported by lubricating oil for a fine-motion stage. *Precision Engineering*, 36(1), 77-83.

Positioning control performance of a rotary switched reluctance actuator (SRA) using modified PID control scheme

Siau Ping Tee[1], Mariam Md Ghazaly[1,*], Chin Kiat Yeo[1], Fawwaz Nadzmy[1], Shin Horng Chong[1], Zulkeflee Abdullah[2]

[1)] Center for Robotics and Industrial Automation (CeRIA), Fakulti Kejuruteraan Elektrik, Universiti Teknikal Malaysia Melaka, Hang Tuah Jaya, 76100 Durian Tunggal, Melaka, Malaysia.
[2)] Fakulti Kejuruteraan Pembuatan, Universiti Teknikal Malaysia Melaka, Hang Tuah Jaya, 76100 Durian Tunggal, Melaka, Malaysia

[*]Corresponding e-mail: mariam@utem.edu.my

Keywords: Rotary switched reluctance actuator; positioning control; modified PID controller

ABSTRACT – This research discusses on the positioning control performance of a rotary switched reluctance actuator (SRA). In this research, the positioning control of the rotary SRA is achieved by implementing the modified PID control scheme. The procedures to construct the linearizer unit is the key elements in the modified PID control scheme. This paper emphasizes on the positioning control performances between the modified PID with the conventional PID. The findings showed that modified PID controller with linearizer unit demonstrated an improved performance, i.e.: at position 74.5°, error is completely eliminated, overshoot and settling time is improved by 81.4% and 76.2%, respectively.

1. INTRODUCTION

A switched reluctance actuator (SRA) is a type of electromagnetic stepper actuator that is gaining approval for its simple and robust design and its ability of exceeding high-speed operation [1-3]. SRA has gained control over permanent magnet actuators due to the fact that its material construction is relatively low cost compared to the expensive and rare permanent magnets. It is well known that the SRA is a highly non-linear characteristic actuator, thus it is particularly difficult to control its position. At present, there are several control methods proposed and established for motion control of linear SRA [2]. However, for rotary SRA they are fairly limited and are mostly involved in model-based control which are highly dependent on the system's modelling [3]. As an option for a much simpler controller, conventional PID controller is a decent option [4]. However, the PID controller is not designed to control a non-linear system. Therefore, this paper discussed the implementation of a modified PID controller for evaluating the positioning performance of an SRA, where the modified PID controller is an improved version of the conventional PID controller.

2. METHODOLOGY

To evaluate the positioning control performance of a rotary switched reluctance actuator (SRA) using modified PID control scheme, several experimental works are evaluated using the prototype shown in Figure 1. Figure 2 shows the block diagram of modified PID controller. The system consists of PID controller, Linearizer unit, and an anti-windup unit. The switching mechanism plays an important role which decides the correct activation of the SRA excitation phase current (Phase A, B and C). Different phases are activated when specified conditions are fulfilled based on the rotor current position. The anti-windup was implemented to avoid the saturation of PID signal due to the integral term.

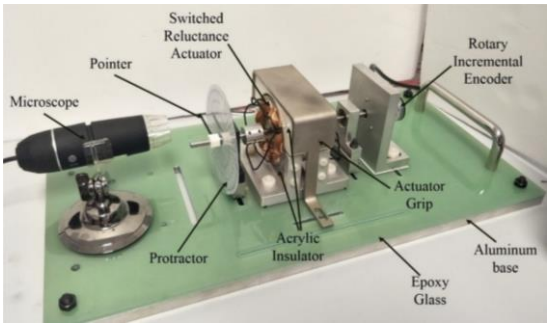

Figure 1 Rotary SRA prototype.

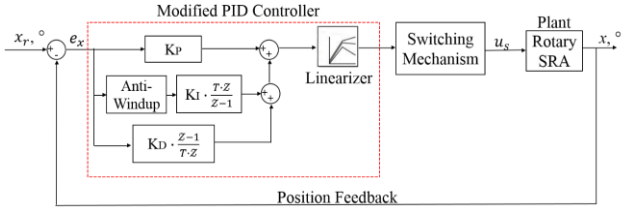

Figure 2 Block diagram of modified PID controller.

Since SRA has a highly non-linear characteristic, thus the presence of the linearizer unit is to compensates for the non-linear current-displacement relationship of SRA system. Figure 3 shows the current-displacement relationship used to construct the linearizer unit for Phase A. Each phase has its own Linearizer unit. Using a customized waveform which consist of combination of positive and negative step signal shown in Figure 4, the residue magnetic flux in rotary SRA can be discharged.

3. RESULTS AND DISCUSSION

To evaluate the effectiveness of the modified PID controller, the SRA is evaluated at reference position 74.5°. The specific positions are tested which includes decimal specific positions to assess the robust performance of the controllers. The controller parameters for both conventional PID controller and modified PID controller is shown in Table 1. Figure 5 shows the point-to-point positioning performances of

the SRA using modified PID controller and the conventional PID controller. The conventional PID controller is validated as a comparative comparison. It can be depicted that the PID controller showed difficulties in achieving positions that are close to the fully aligned position at 74.5°. From Table 2, the modified PID controller displayed an excellent performance in compared to PID controller where the positioning error is 100% eliminated, overshoot and settling time is improved by 81.4% and 76.2%, respectively.

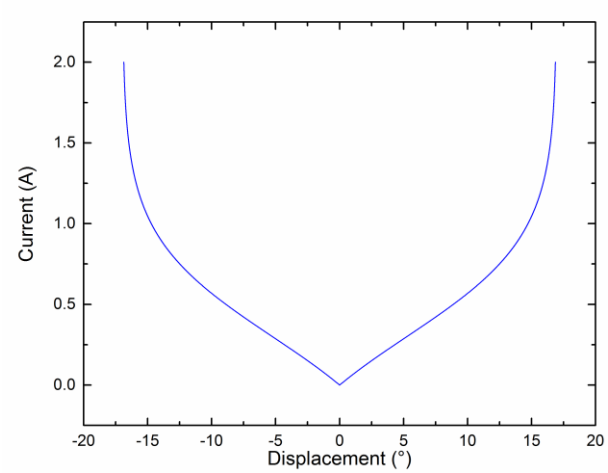

Figure 3 Current-displacement relationship to construct linearizer block for Phase A.

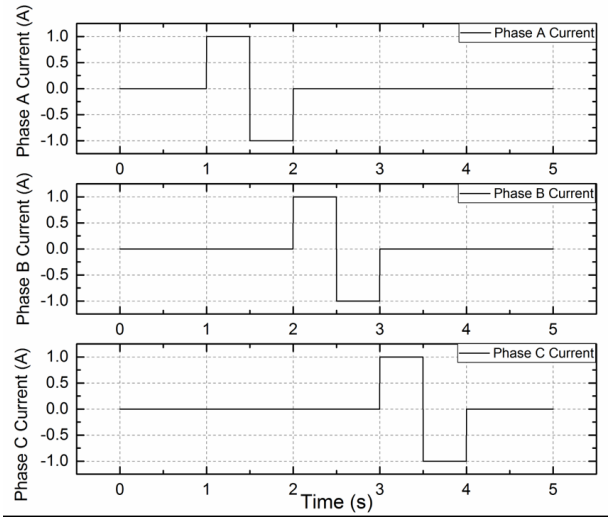

Figure 4 Customized waveforms for discharge of magnetic flux in SRA.

Table 1 Controller parameters for conventional PID and modified PID controllers.

	Modified PID	**Conventional PID**
K_P (°)	2.02	0.3
K_I (°s^{-1})	22	3.28
K_D (°s)	0.07	0.01

4. CONCLUSION

In conclusion, the positioning control performance of a rotary switched reluctance actuator (SRA) using modified PID control scheme is validated. It shows that the linearizer unit and anti-windup elements are able to greatly improve the positioning performance of the rotary SRA. Future works includes the improvement of the linearizer unit using high resolution encoder and the inclusion of system's frictional force for micro-positioning and trajectory tracking.

Table 1 Transient parameters for modified PID and PID controller at reference position 74.5°.

Parameters	**Modified PID**	**PID**	**Improvement (%)**
Steady-state Error (°)	0.00	7.90×10^{-1}	100.0
Overshoot (%)	3.56	1.91×10^{1}	81.4
Settling Time (s)	1.73×10^{-1}	7.24×10^{-1}	76.2

ACKNOWLEDGEMENT

The authors wish to express their gratitude to Motion Control Research Laboratory (MCon Lab), Center for Robotics and Industrial Automation (CeRIA) and Universiti Teknikal Malaysia Melaka (UTeM) for supporting the research and publication. This research is supported by Universiti Teknikal Malaysia Melaka grant no. JURNAL/2018/FKE/Q00006, Center for Robotics and Industrial Automation (CeRIA) and Center for Research and Innovation Management (CRIM).

REFERENCES

[1] Yusri, I., Ghazaly, M. M., Alandoli, E. A. A., Rahmat, M. F., Abdullah, Z., Ali, M. A. M. & Ranom, R. (2016). Force optimization of the permanent magnet switching flux (PMSF) and switching reluctance (SR) actuators using finite element analysis. *Proceedings of Mechanical Engineering Research Day 2016*, 2016, 1-2.

[2] Wang, S. Y., Liu, F. Y. & Chou, J. H. (2016). Design on sliding mode controller with adaptive fuzzy compensation for switched reluctance motor drive systems. *2016 International Symposium on Computer, Consumer and Control, Xi'an, China,* 2016, 239-242.

[3] Kojima, T. & De Doncker, R. W. (2015). Optimal torque sharing in direct instantaneous torque control of switched reluctance motors. *IEEE Energy Conversion Congress and Exposition, Montreal, Canada,* 2015, 327-333.

[4] Veena, N. D. & Raghuram, N. L. (2017). Minimization of torque ripple using ditc with optimum bandwidth and switching frequency for srm employed in electric vehicle. *International Conference on Smart Grids, Power and Advanced Control Engineering, Bangalore, India,* 2017, 143-148.